Journal of African Earth Sciences 183 (2021) 104327

Contents lists available at ScienceDirect

Journal of African Earth Sciences

journal homepage: www.elsevier.com/locate/jafrearsci

Paleoweathering, Provenance and tectonic setting of gold-bearing neoproterozoic rocks from the Atacora Structural Unit, Pan-African Dahomeyide belt, northwestern Bénin

Fatchéssin Bruno Adjo [a,c,*], Prosper M. Nude [b], Luc Glodji Adissin [c], Anthony Temidayo Bolarinwa [a], Bertrand Anagonou [c]

[a] Department of Geosciences, Pan-African University Life and Earth Sciences Institute, University of Ibadan, Nigeria
[b] Department of Earth Science, University of Ghana, Legon, Ghana
[c] Department of Earth Sciences, University of Abomey-Calavi, Calavi, Bénin

ARTICLE INFO

Keywords:
Atacora Structural Unit
Natitingou
Palaeoweathering
Provenance
Tectonic setting

ABSTRACT

The Atacora Structural Unit (ASU) is part of the Pan-African belt located in Northwestern Bénin Republic. It consists of metasedimentary rocks of greenschist facies and composed of quartzites, mica schists and chlorite-sericite-quartz schists. A petrochemical study of these rock types was undertaken, geared at inferring their paleoweathering, provenance and tectonic setting. Texturally, the rocks are, medium to coarse-grained with angular to rounded clasts. Detrital component statistics classified them as sublitharenite/quartzarenite. Geochemically, they can be classified as arkose/subarkose and sublitharenite rocks. The average values for PIA, CIA, and CIW for the quartzites, mica schists and schists range from 75% to 98%, reflecting an intensive degree of chemical weathering. The LREE enrichment (LaN/YbN = 9.56), negative europium anomaly (Eu/Eu* = 0.77), and fractionated HREE patterns of chondrite-normalized, are comparable to melts generated from crustal continental materials. The geochemical studies show that the studied rocks were sourced from ancient quartzose sedimentary rocks. Trace element ratios Cr/Th, Zr/Sc, Th/Sc, Th/Co and La/Th and rare earth elements of the source components indicate that these mature materials were chiefly derived from felsic rocks, though the involvement of basic rocks (basalts) cannot be ruled out. Chondrite-normalized REE patterns indicate that the metasedimentary rocks are sourced from pre-existing sedimentary rocks in the ASU, which rocks were mainly derived from the Dahomeyide basement and probably from the Amazonia craton. The major and trace elements discriminant diagrams suggest these metasediments were deposited in a passive-margin setting, though continental island arc setting signature was also identified.

1. Introduction

Geochemical studies are widely used to evaluate the chemical composition of the crustal protolith material and the relative enrichment of the constituents of clastic sedimentary rocks such as major detrital elements, useful metals and metamorphic phases (Roser, 2000). The investigation of bulk rock major, trace and rare earth elements (REEs) concentrations, can be useful in the discrimination of the tectonic setting, provenance, and evolution of the continental crust. They can also be used to constrain the source components and evolution of clastic metasediments (Bhatia, 1985; Condie, 1991, 1993, 1993; McLennan et al., 1993; Nesbitt and Young, 1996; Gabo et al., 2009; Armstrong-Altrin, 2009; Oghenekome et al., 2016). The chemical composition of fine grained sedimentary rocks such as shale is believed to be the most suitable for the discrimination of the provenance and tectonic context due to the homogeneity of sediments before their deposition, post-depositional impermeability, and the high concentration of trace elements (Condie, 1993; Cox and Lowe, 1995; McLennan et al., 2000). Rare earth elements (REEs) and some trace elements such as Hf, Sc, Th, Zr display usually minor concentrations in natural waters and are conveyed mostly abundantly during the sedimentary process from the source rocks to siliciclastic sediments (Condie, 1991; Armstrong-Altrin, 2009). The moderate distribution of these immobile elements in different types of rocks allow to deduce the probable input of

* Corresponding author. Pan-African University Life and Earth Sciences Institute, University of Ibadan, Nigeria
E-mail address: afab8213@gmail.com (F.B. Adjo).

https://doi.org/10.1016/j.jafrearsci.2021.104327
Received 20 May 2020; Received in revised form 26 June 2021; Accepted 13 July 2021
Available online 14 July 2021
1464-343X/© 2021 Elsevier Ltd. All rights reserved.

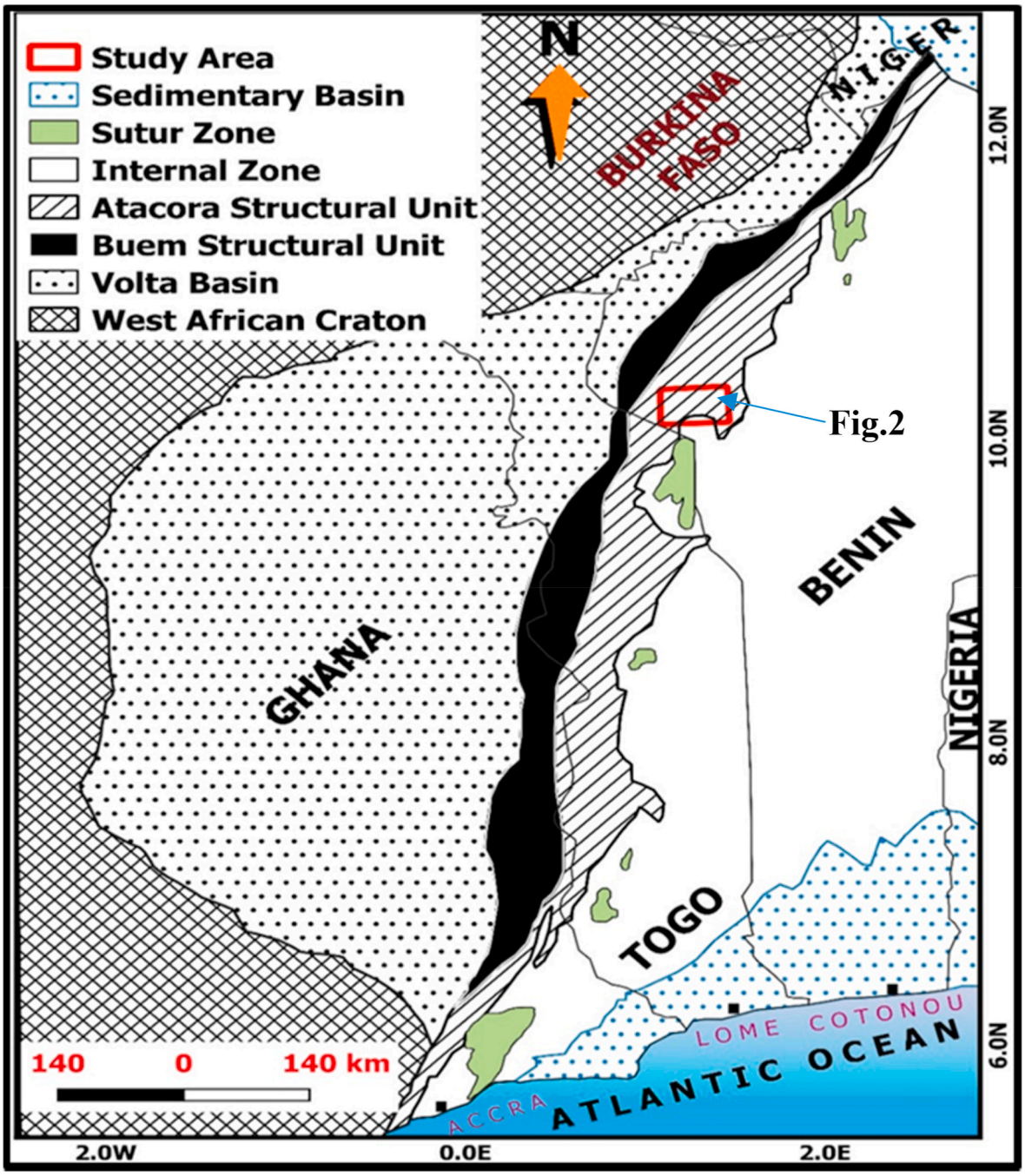


Fig. 1. Regional geological map, showing main components of Pan-African Dahomeyides belt and the study area, modified after Affaton et al. (1991).

basic and felsic sources in sedimentary rocks (Wronkiewicz and Condie, 1990).

Though the geochemical characteristics of classic metasedimentary rocks have been pivotal in decrypting tectonic environment and provenance, geochemical studies on the Atacora Structural Unit (ASU) at the Bénin side is undocumented. Comparatively, the ASU on the Republic of Ghana side (where it is known as the Togo Structural Unit, TSU) and in the Republic of Togo has been well studied and documented. Kalsbeek et al. (2012), using U–Pb zircon data on quartzite sample of the ASU, indicated that this lithology may be comparable to the sedimentary materials of the Lower Volta basin which cover parts of the eastern margin of the West African Craton. Geochemical studies by Anani et al. (2019), on metasedimentary rocks of the TSU in Ghana suggest that the rocks were mainly from recycled sedimentary sources and the provenance features are comparable to that of the lower sequence of Volta basin with passive continental margin chemical characteristics.

The Natitingou area located in the ASU (Fig. 1) hosts good exposures of metasedimentary rocks. This area is known for its historical artisanal gold mining sites with gold production within the Pan-African Dahomeyides external zone (Adjo et al., 2019, Adjo et al., 2021). The chemical composition of these rocks has remained poorly documented, hence their source and tectonic setting remain unclear.

This study aims to document the petrochemistry of the ASU rocks in northwestern Bénin by assessing their source characteristics, provenance, and tectonic context as well their weathering condition during Neoproterozoic time. This is relevant in reconstructing the paleogeography of the Natitingou area which singularly hosts abundant gold in the ASU of the Dahomeyides belt.

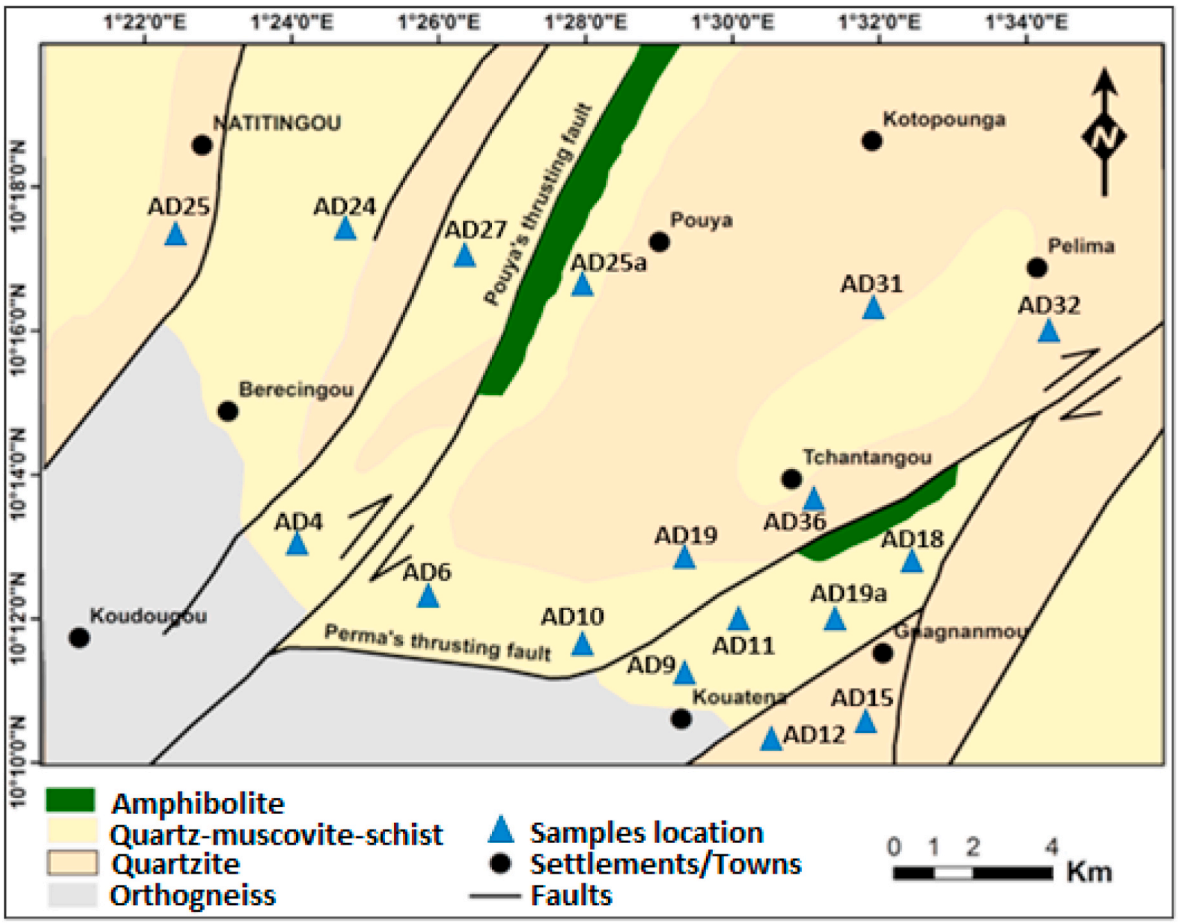


Fig. 2. Geological map of the study area with sample locations.

2. Geological setting

The Pan African orogenic Dahomeyides belt formed as a result of the continental collision between the eastern margin of the West African Craton (WAC) and the Benin-Nigerian shield after the closure of a subduction event around 0.6 Ga years ago (Bessoles et al., 1980; Caby, 1989; Affaton et al., 1991; Ganade et al., 2016). The belt has a well-organized orogenic architecture with its main three litho-structural zones (Fig. 1) i. e., from West to East, the external zone, the suture zone and the internal zone or the Benino-Nigerian geological province (Affaton et al., 1991; Deynoux et al., 2006; and therein references). These zones are separated by thrust contacts and each one constitutes a thrust sheet. The internal nappes mainly composed of granitic gneiss and migmatitic rocks; (2) the suture zone (intermediate nappes) made up of SSW–NNE elongated eclogites, pyroxenites, metanorites and granulite bodies parallel to the Pan African structural trend; and (3) the external nappes interpreted as the deformed edge of the WAC and its covers rocks comprising the Buem and Atacora (Togo) Structural Units. The deformed edge of the WAC constitutes the basement Dahomeyan external unit (basement complex) and made up of meta granites, granodiorites, amphibolites and varied gneisses known in Ghana as Ho gneisses, and in Togo as Kara and Palime-Amlame gneisses (Affaton et al., 1991; Attoh et al., 1997; Agbossoumondé et al., 2007). Previous works interpreted these rocks as remobilized rocks derived from partial melting of thickened Archean lower crust during the Eburnean Orogeny at ~2.1 Ga (Agbossoumondé et al., 2007; Aidoo et al., 2020). Deformed alkaline rocks and carbonatite occur at the sole thrust of the suture zone and the basement complex (Attoh and Nude, 2008; Nude et al., 2009). The Buem Structural Unit (BSU) consists of succession of massive arkoses and a thick pile of shales, siltstones mudstones interbedded with chert, limestones, mafic and felsic volcanics as well serpentinized ultramafic rocks. It is regarded as the westernmost unit of the Dahomeyides external nappes and thrusts to west on the Volta Basin sediments, which corresponds to the foreland of the belt. The Atacora Structural Unit (ASU) is a range of mountains consisting of quartzites hills and phyllites recrystallized in greenschists to amphibolite facies conditions (Affaton et al., 1991; Castaing et al., 1993; Adjo, 2021). The best exposures of the ASU occur in the Natitingou area which is predominantly made of siliciclastic metasedimentary rocks (Adjo, 2021; Adjo et al., 2021a). These latter exhibit a polyphase deformation, reflecting orogenic and collisional effects produced through the Pan-African event (Adjo, 2021; Adjo et al., 2021b).

U–Pb zircon data acquired on two quartzite samples (one from the ASU and one from the Togo Structural Unit) have detrital zircon signatures compatible with the Volta Basin lower units (Ganade et al., 2016). Geochronology data on the quartzites of the Togo Structural Unit (TSU), Kalsbeek et al. (2008); Kalsbeek and Frei (2010) have suggested that this unit might be also compared to the Kwahu/Bombouaka Group of the Volta Basin.

3. Materials and methods

For this study, seventeen (17) fresh representative samples composed of mica schists ($n=9$), quartzites ($n=4$), and chlorite sericte-quartz schists ($n=3$) were selected among samples collected during the geological mapping within the Natitingou area (Fig. 2). Thin sections of all rock samples were prepared at the Geology Department, Obafemi Awolowo University, Ile-Ife, Nigeria and were studied under the petrographic microscope to determine their texture, mineral phases and paragenesis, and alteration phases. The seventeen selected samples were

Table 1
Modal composition of the seventeen selected quartzites and mica schist samples from the Natitingou area. (Qm: mono-crystalline quartz; Qp: poly-crystalline quartz; Qt: total quartz (Qt = Qp + Qm); P plagioclase grains, K potassium feldspars, F total feldspar grains (F=K + P), L: total lithics; M: mica; G: Garnet; C: Chlorite).

Lithology	Sample	Qm	Qp	Qt	P	K	F	L	M	C	G	TOTAL
Quartzite	**AD4**	81.0	10	91.0	0	0	0	1	8	0	0	100
	AD6	90.0	3.0	93.0	2	2.5	4.5	1	1.5	1	0	100
	10 CE	83.0	7.0	90.0	2	3	5	2	2	1	0	100
	12 CE	89.0	3.0	92.0	3	2	5	2	1	0	0	100
	19 CE	85.0	8.0	93.0	1	3	4	0	2	1	0	100
	24 CE	82.5	5.0	87.5	0	0	0	1.5	10	1	0	100
	25 CE	81.0	4.0	85.0	3.5	2	5.5	2	5	2	0	100
	31 CE	83.0	2.0	85.0	3	3	6	1	6	2	0	100
	32 CE	81.5	4.0	85.5	2	4.5	6.5	0	7	1	0	100
Mica schist	**AD9**	79	2	81	0	2	2	2	13	2	0	100
	11 CE	74.5	0.5	75	1.5	1.5	3	3.5	15.5	3	0	100
	15 CE	77.5	1.3	78.8	1	1	2	0	15	4.2	0	100
	AD25a	67	1	68	2.5	1.5	4	8	17	4	0	100
	27 CE	74	2	76	0	1	1	4	14	5	0	100
Schist	**18 CE**	65	0	65	1	1	2	5	8	12	8	100
	AD19a	73	3	76	1	1.5	2.5	0.5	10	11	0	100
	36 CE	62.5	2	64.5	2	2	4	9	7.5	10	5	100

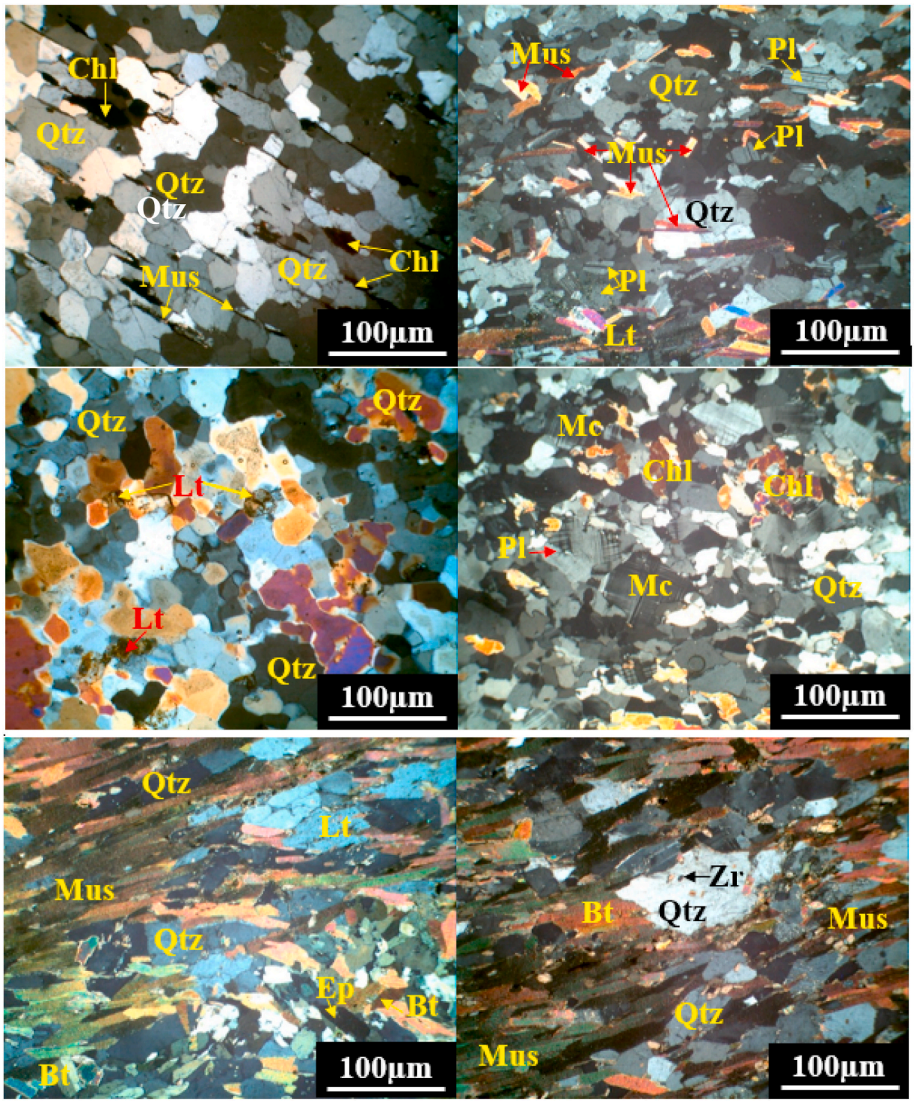


Fig. 3. Microphotographs of the ASU metasedimentary rocks showing a texturally matured grains (**a**–**d**) in quartzites; (**e**–**f**) in schistose rocks. [Qtz– quartz; Mus– muscovite; Mc– microcline; Pl– plagioclase; Bt– biotite; Chl– chlorite; Ep– epidote; Lt– lithic fragment].

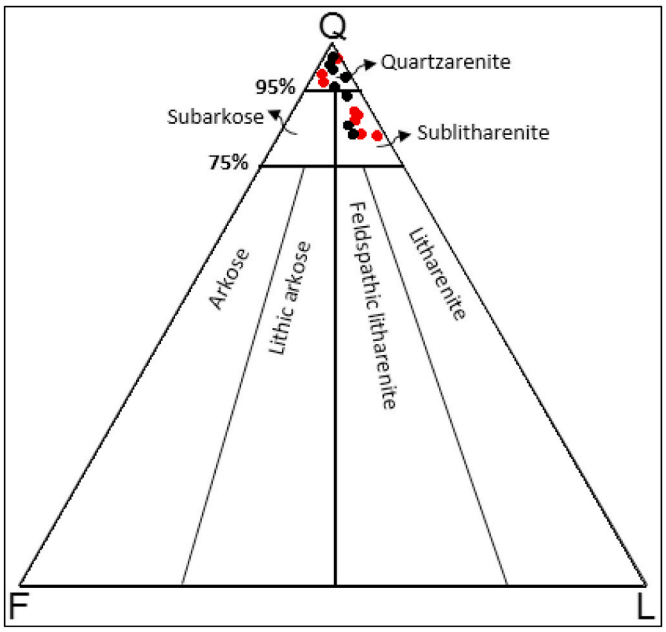


Fig. 4. Petrographic classification of the ASU studied rocks plotted on Q-F-L diagram after Folk (1980). [Q: total quartz; F: total feldspar; L: lithic fragments; Circle red: quartzites; circle black: schist and micaschist]. (For interpretation of the references to colour in this figure legend, the reader is referred to the Web version of this article.)

crushed, pulverized to below 200 mesh, packaged and sent to Bureau Veritas Commodities Ltd (ACME Laboratories), Vancouver, Canada. 0.2g of each sample were mixed with lithium metaborate/tetraborate and fused at 1025 °C in a furnace for their decomposition. Inductively-Coupled Plasma Emission Spectrophotometry (ICP-ES) with an analytical precision ranging between 0.002 and 0.04 percent was used to assess the major oxides compositions and Loss on Ignition (LOI) of the rocks. The weight difference after ignition at 1025 °C was used to calculate the LOI percentage while Inductively-Coupled Plasma-Mass Spectrometer (ICP-MS) with 0.01–0.5 ppm Detection limits for all trace elements was used to analyse trace and rare-earth elements in accordance with the Code LF202 analytical package (ACME Laboratories). The reference materials such as STD DS11, STD GS311-1, STD GS910-4, STD OREAS262, STD GBM309-15, and STD SO-19 were used for the analyses. The analytical data obtained were grouped based on their chemical similarities.

Various discriminatory parameters and diagrams of the major and trace elements were used to characterize the provenance and tectonic environment. The binary plots of Log Na_2O/K_2O against log SiO_2/Al_2O_3 (Pettijohn, 1975) and the ternary diagram (Q-F-L) of Folk (1980) were used in classifying the rocks. The ternary plot (Nesbitt and Young, 1982, 1984) expressed as [Al_2O_3-(CaO*+Na_2O)–K_2O] as well the formulas for chemical index of weathering (CIW), chemical index of alteration (CIA), and plagioclase index of alteration (PIA) were valuable in the evaluation of the weathering degree. In the formulas, CaO* is the quantity of CaO amalgamated to the silicate portion of the rock.

4. Results

4.1. Petrography

As stated above, the metasedimentary rocks studied in this paper are quartzites, mica schists and chlorite-sericite-quartz schists. Their petrographic analysis were done to classify the protolith of rocks and understand the sedimentary histories. Modal compositions of representative medium to coarse-grained textured quartzites and schistose rocks are shown in Table 1.

4.2. Quartzite

The analysed quartzites are texturally mature. The framework grains are dominated by monocrystalline and polycrystalline quartz, muscovite, K-feldspar, plagioclase, lithic fragments, and chlorite, in decreasing order of abundance (Fig. 3a–d). The subangular to subrounded quartz grains are the dominant components, with monocrystalline quartz (Qm) ranging from 81% to 90% and by volume and polycrystalline quartz (Qp) ranging from 2 to 10% by volume (Table 1). Most of monocrystalline quartz are undulatory (Fig. 3a and c). Polycrystalline quartz are composed more than two crystals with little curved intercrystalline borders. The feldspar content is low (4–6.5%; Table 1) and composed of microcline and oligoclase (Fig. 3b and d). Lithic fragments (mainly sedimentary) account for 1%–2% and composed of chert while the muscovite content range from 1% to 10% by volume. Minor amounts (2%) of chlorite was also observed According to the classification scheme of Folk (1980) and based on the modal analysis, the quartzites of the ASU can be classified as quartzarenites and sublitharenite (Fig. 4).

4.3. Mica schist and chlorite-sericite-quartz-schist

Textural analysis shows that the framework of the schistose rocks consist of quartz, muscovite, biotite, microcline, plagioclase, chlorite, garnet (Fig. 3e and f). Accessories minerals include pyrite, ilmenite, rutile, epidote, sphene and zircon. The percentages of total quartz grains (Qt), total feldspar grains (F) and total lithic fragments (L) are 64.5–81% (Av. 73%), 1–4% (Av. 2.4%) and 12–17% (Av. 4.2), respectively (Table 1). The percentages of monocrystalline quartz grains (Qm), polycrystalline quartz grains (Qp), micas, K-feldspar and plagioclase grains are 62.5–79%, 0–3%, 7.5–17%, 1–2% and 0–2.5%, respectively, with average percentages of 71.6%, 1.5%, 12.5%, 1.44%, and 1,12%, respectively. (Table 1). Monocrystalline quartz are both non-undulose and undulose. Some quartz grains and plagioclase contain inclusions of heavy minerals such as zircons (Fig. 3f). Micas are composed of muscovite and biotite with a dominance of muscovite over biotite. Chlorite probably derived from biotite accounts for 2–12% while garnet occupy 0–8% by volume. From the detrital modes, the studied schistose rocks have also the composition of quartzarenites and sublitharenites as illustrated in (Fig. 4).

4.4. Geochemistry

The results of the major and trace elements analysis of the ASU metasedimentary rocks are presented in Table 2.

4.4.1. Major elements

The results of the analysis show a large variation in the content of the major elements.

The quartzite samples are composed of: SiO_2 (88.27–94.03 wt %), Al_2O_3 (2.02–6.38 wt %), TiO_2 (0.07–0.32 wt%), Fe_2O_3 (0.85–1.58 wt%), and MgO (0.10–0.17 wt%). K_2O contents range between 0.54 and 1.54 wt% while sodium oxide (Na_2O) contents range from 0.10 to 0.18 wt%. The contents of CaO, P_2O_5 and MnO are mostly less than 0.1 wt% (Table 2). The graph of Pettijohn (1975) revealed that these quartzites can be characterised as subarkose to sublitharenite (. 5a).

The schistose rocks have the following compositional ranges: 61.28 to 88.87 wt % of SiO_2, 4.28 to 17.55 wt% of Al_2O_3, 2.68 to 10.5 wt% of Fe_2O_3, 0.13 to 2.55 wt % of MgO, 0.01 to 0.88 wt% of CaO, 0.12 to 0.53 wt% of Na_2O, 0.68 to 5.27 wt% of K_2O, 0.3 to 1.41 wt% of TiO_2, 0.02 to 0.23 wt% of P_2O_5, and 0.01 to 0.11 wt % of MnO (Table 3). As presented in Fig. 5a, the chlorite-sericite-quartz schist and mica schist show the composition of arkose.

The analysed rocks are rich in quartz as indicated by their high silica content with an average of 90.61 wt% in quartzite and 74.77 wt% in the

Table 2
Major (wt %) and trace elements (ppm) composition of quartzites from the Natitingou area.

Lithology	Quartzite								
Sample	AD4	AD6	10 CE	12 CE	19 CE	24 CE	25 CE	31 CE	32 CE
SiO_2 (W. %)	88.27	94.03	93.92	92.26	93.14	86.68	92.86	86.98	87.39
TiO_2	0.23	0.07	0.13	0.16	0.09	0.32	0.14	0.27	0.32
Al_2O_3	5.79	2.14	2.02	2.95	3.02	6.38	2.53	6.32	5.98
Fe_2O_3	1.16	0.97	0.85	1.58	1.73	1.32	1.66	1.29	1.32
MgO	0.15	0.11	0.14	0.12	0.10	0.16	0.13	0.17	0.16
CaO	0.03	0.10	0.08	0.09	0.09	0.06	0.11	0.05	0.06
Na_2O	0.15	0.13	0.12	0.13	0.11	0.18	0.10	0.16	0.17
K_2O	1.33	0.54	0.69	0.69	0.70	1.52	0.66	1.54	1.51
P_2O_5	0.04	0.05	0.04	0.04	0.04	0.05	0.06	0.05	0.04
MnO	<0.01	<0.01	0.01	<0.01	0.01	0.02	0.01	0.02	0.01
Cr_2O_3	0.005	0.003	0.005	0.004	0.004	0.004	0.003	0.005	0.004
LOI	2.80	1.80	1.90	2.00	2.10	3.20	2.00	3.10	3.00
Total	99.97	99.99	*99.98*	99.98	*99.99*	99.94	*99.98*	99.96	99.96
Log (SiO_2/Al_2O_3)	1.18	1.64	1.56	1.50	1.14	1.13	1.16	1.49	1.67
Log (Na_2O/K_2O)	−0.95	−0.62	−0.82	−0.72	−0.98	−0.93	−0.95	−0.80	−0.76
PIA	96.75	92.39	92.39	95.59	95.02	96.41	94.46	96.74	96.73
CIA	79.65	76.11	77.49	78.79	77.85	78.95	78.86	78.89	79.55
CIW	97.48	94.20	93.83	96.59	96.00	97.24	96.60	97.32	97.42
Trace elements (ppm)									
Ba	122	37	27	65	26	226	27	118	45
Ni	20	20	20	20	19	20	20	19	19
Sc	5.0	2.0	2.0	3.0	6.0	6.0	2.0	2.0	3.0
Be	2.0	10	7.0	8.0	8.0	3.0	9.0	3.0	3.0
Co	2.6	1.4	1.5	1.3	1.3	4.8	1.4	2.9	0.7
Cs	0.9	0.7	0.5	0.8	0.5	1.1	0.6	0.9	20.8
Ga	6.3	1.6	0.9	2.6	1.0	6.2	0.8	4.9	25.8
Hf	2.5	1.4	0.8	2.0	0.8	5.9	0.9	1.8	1.3
Nb	3.4	1.7	1.1	2.2	2.1	4.4	1.0	2.6	31.2
Rb	37	16.1	12.5	22.1	12.4	43.6	12.7	33.6	41.7
Sn	2.0	2.0	2.0	2.0	2.0	3.0	1.0	2.0	2.0
Sr	23	14.6	9.1	13.9	9.1	31	9.4	19.1	18
Ta	0.3	0.2	0.2	0.3	1.6	0.5	0.1	0.2	5.8
Th	3.5	1.6	1.0	2.3	0.9	4.9	0.9	2.8	1.3
U	0.6	0.3	0.1	0.3	0.2	1.1	0.2	0.4	2.1
V	15	9.0	8.0	9.0	9.0	20	8.0	16	8.0
W	2.3	1.0	0.7	1.5	0.9	1.8	0.7	18.8	1.7
Zr	104.8	50.2	30.7	68.4	29	220.1	34.1	70.2	15.5
Y	11.4	6.3	4.0	7.2	3.9	14.2	4.3	9.3	6.0
Mo	0.9	1.3	3.3	1.1	2.8	0.8	2.6	2.9	0.3
Cu	20.8	27.5	23.5	27	21.1	19.1	21.4	19.5	7.3
Pb	0.7	0.9	1.2	0.9	1.1	2.9	0.9	1.1	2.2
Zn	5.0	7.0	7.0	7.0	6.0	8.0	8.0	6.0	4.0
As	1.3	1.9	2	1.7	1.5	1.2	2.1	1.7	0.5
Au (ppb)	4.4	43.2	29	18.9	13.7	464	38.6	2.9	0.5

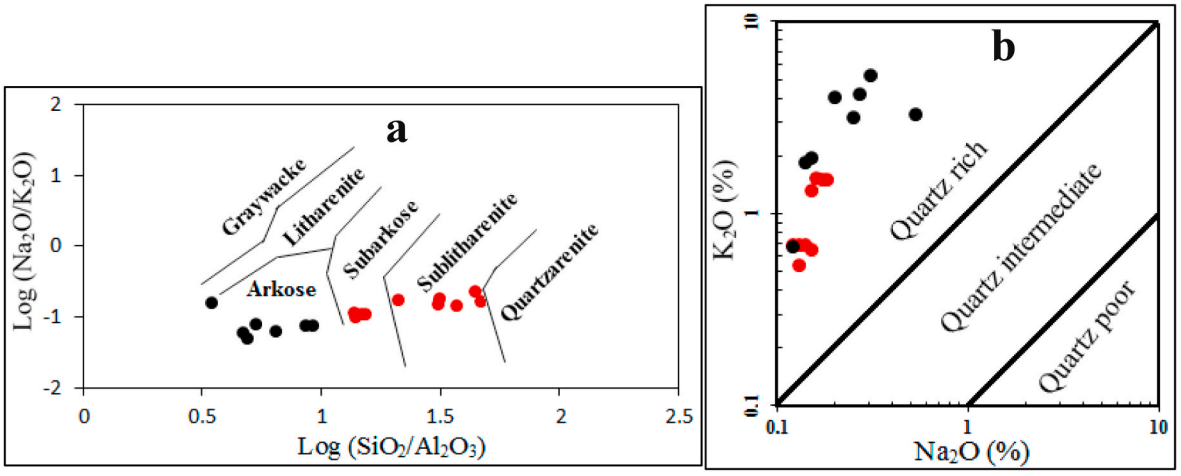


Fig. 5. Geochemical classification of the ASU studied rocks, including **(a)** Log Na_2O/K_2O against log SiO_2/Al_2O_3 plot after Pettijohn (1975); (**b**) K_2O (W%) against Na_2O (W%) plot after Crook (1974). [Circle red: quartzites, circle black: schist and micaschist]. (For interpretation of the references to colour in this figure legend, the reader is referred to the Web version of this article.)

Table 3
Major (wt %) and trace elements (ppm) composition of mica schist and schist from the Natitingou area.

Lithology	Micaschist					Schist		
Sample	AD9	11 CE	15 CE	AD25a	27 CE	18 CE	AD19a	36 CE
SiO_2 (W. %)	88.87	81.12	81.83	61.28	70.92	69.04	77.92	67.2
TiO_2	0.30	0.53	0.54	0.92	0.91	1.01	0.59	1.14
Al_2O_3	4.28	9.4	8.89	17.55	13.35	14.62	12.07	13.77
Fe_2O_3	2.68	4.38	4.31	6.96	7.38	7.34	3.31	10.25
MgO	0.13	0.19	0.18	2.55	0.38	0.59	0.23	0.47
CaO	0.18	0.01	<0.01	0.88	<0.01	0.07	<0.01	0.18
Na_2O	0.12	0.15	0.14	0.31	0.27	0.53	0.25	0.2
K_2O	0.68	1.97	1.84	5.27	4.23	3.27	3.15	4.06
P_2O_5	0.05	0.02	0.02	0.23	0.01	0.04	0.02	0.08
MnO	0.04	<0.01	0.01	0.10	0.01	0.01	<0.01	<0.01
Cr_2O_3	0.005	0.002	0.002	0.013	0.022	0.007	0.002	0.004
LOI	2.60	2.10	2.20	3.60	2.40	3.30	2.40	2.40
Total	99.95	99.95	99.94	99.83	99.94	99.87	99.94	99.84
Log (SiO_2/Al_2O_3)	1.32	0.94	0.96	0.54	0.73	0.67	0.81	0.69
Log (Na_2O/K_2O)	−0.75	−1.12	−1.12	−0.79	−1.10	−1.23	−1.19	−1.31
PIA	96.69	98.02	98.05	97.42	97.12	95.53	97.27	97.95
CIA	84.20	81.60	81.78	75.82	74.79	79.36	78.02	76.36
CIW	97.20	98.43	98.45	98.18	98.02	96.49	97.97	98.55
Trace elements (ppm)								
Ba	81	249	238	1104	676	200	324	526
Ni	20	20	20	49	28	37	20	30
Sc	3.0	11	10	16	19	16	13	24
Co	6.5	1.9	2.2	17.2	4.5	13.8	2.1	10.3
Cs	1.5	2.0	2.3	6.3	1.9	3.5	2.5	10.7
Ga	4.0	9.4	9.7	22.2	13.5	15.7	12.9	20.5
Hf	4.8	4.5	5.2	6.3	2.9	9.6	5.7	9.6
Nb	6	5.9	6.6	20.9	4.4	12.6	7.1	10.4
Rb	30.9	69.4	68.3	168.6	53.9	91.7	81.2	135.2
Sn	4.0	1.0	1.0	3.0	1.0	3.0	1.0	2.0
Sr	17.1	20.2	20.1	85.7	39.5	75.3	44.5	108.2
Ta	0.6	0.4	0.5	1.4	0.3	1.0	0.6	0.7
Th	5.4	8.3	8.7	20.3	3.8	16.3	7.1	9.4
U	1.5	1.2	1.3	2.4	0.6	2.3	1.3	2.0
V	20	16	18	87	81	28	29	63
W	0.8	3.3	3.6	3.2	2.4	6.4	13.9	1.8
Zr	179.5	182.2	194	230.4	108.2	366.3	222.7	376.4
Y	14.4	32	30.4	23.8	12.9	61.3	27.3	63.9
Mo	2.5	<0.1	<0.1	<0.1	<0.1	0.5	<0.1	<0.1
Cu	24.5	2	1.8	33.7	2.9	14	3.1	2.4
Pb	5.2	2.2	0.5	9.2	1.3	0.9	1.3	1.9
Zn	16	1.0	2.0	71	1.0	4.0	2.0	3.0
Ni	5.7	0.5	0.4	35.5	0.8	1.7	0.2	2.4
As	2.1	1.5	1.3	0.7	<0.5	1.5	11.3	<0.5
Au (ppb)	8.8	1.1	<0.5	49.4	<0.5	15.3	9587	<0.5

schistose rocks. The plot of Na_2O against K_2O (Fig. 5b), indicate these ASU metasedimentary are quartz-rich. The mean content of Fe_2O_3 + MgO is 1.90 wt% which suggests that the samples contain traces of mafic material. The higher Fe_2O_3 concentration in some samples may be related to the presence of magnetite and hematite minerals. The average CaO, Al_2O_3, Na_2O, K_2O contents of these rocks are respectively 0.12 wt %, 7.71 wt %, 0.19 wt % and 2.34 wt %, suggesting an impoverishment of feldspars. However, the rocks have significant amounts of K_2O (mainly in schistose rocks) which could occur through conveyance or due to the modification feldspars in the source area (Tobia and Aswad, 2015). It could also be related to K addition during diagenesis. Similarly, the studied rocks show appreciable TiO_2 content because of the Titanium-rich minerals, for example rutile, ilmenite and sphene.

SiO_2 show strong negative correlation with K_2O, Al_2O_3, Fe_2O_3, TiO_2 and MgO, moderate or weak correlation with Na_2O, CaO and P_2O_5 (Fig. 6a). There is no correlation between MnO and SiO_2. The oxides such as TiO_2, K_2O, Fe_2O_3 and Na_2O show strong positive correlations with Al_2O_3 (Fig. 6b). According to Fedo et al. (1996), elements such as Al_2O_3, TiO_2, K_2O, Fe_2O_3 and Na_2O indicate high weathering level of the source area where Calcium is favourably leached while potassium and magnesium are incorporated in clay minerals. Conversely, MgO, P_2O_5 and CaO show a moderate positive correlation (correlation coefficient R = 0.85, 0.44 and 0.45 respectively) with Al_2O_3. Moreover, increase in the amounts of K_2O with Al_2O_3 (Fig. 6b) indicates that the potassium and aluminium absorption is controlled by the mica, the clay minerals (chlorite and illite) and K-feldspars (microcline) in ASU metasedimentary rocks (Khanehbad et al., 2012; Hu et al., 2015).

4.5. Trace elements

Because of numerous parameters including physical sorting, adsorption, weathering, provenance, metamorphism and diagenesis, trace elements have a complex behaviour during sedimentary processes (Nesbitt et al., 1980; Wronkiewicz and Condie, 1987; Rollinson, 1993). The trace element content of the analysed metasedimentary rock samples show a wide range of concentrations (Tables 2 and 3).

The average value of Large Ion Lithophile Elements (LILE) Ba, Rb, K, Sr and Cs, are 240.64 ppm, 54.76 ppm, 16.65 ppm, 41.23 ppm and 3.38 ppm, respectively. K_2O correlated positively with Ba (r = 0.90), Rb (r = 0.87), Cs (r = 0.70) and Sr (r = 0.82). This indicates that the higher contents of K, Ba, Rb and Sr in the ASU metasedimentary rocks is controlled by K-bearing clay minerals such as muscovite and biotite (McLennan et al., 1993; Rollinson, 1993). High field strength elements (HFSE values of Th/U range widely (3.6–10; Tables 4 and 5) and greater than those of the average Neoproterozoic upper continental crust (UCC) value of about 3.9 (Condie, 1993); the Th/Sc contents varying from 0.2

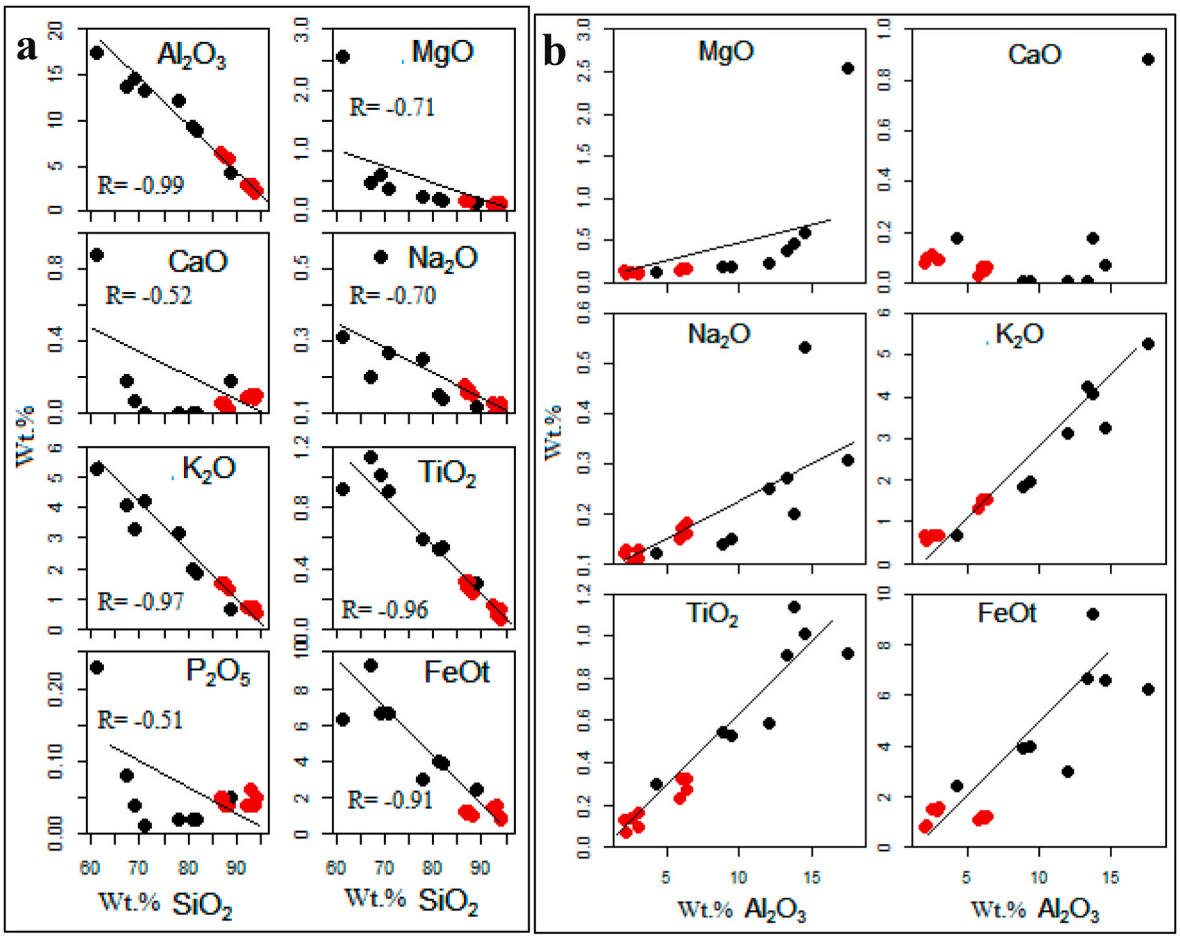


Fig. 6. Major oxides relationships diagrams for the Atacora Structural Unit metasedimentary rocks from Natitingou area. (**a**) Harker variation diagrams, (**b**) Major oxides versus Al_2O_3 diagrams. [In both diagrams, Circle red: quartzites, circle black: schist and micaschist]. (For interpretation of the references to colour in this figure legend, the reader is referred to the Web version of this article.)

to 1.8 are generally above those of the average UCC value of 0.72 (Condie, 1993). The spider diagrams of the ASU metasedimentary rocks compared to UCC (Fig. 7) show parallel signatures with a poor enrichment in some elements and a depletion in the same elements in some samples. However, the concentrations of the trace elements are chiefly below those of the UCC particularly in all quartzite samples (Fig. 7a and b).

The concentrations of base metals, i.e. Ni, Pb, Zn, Cu, and Sn range from 20 to 49 ppm, 0.5–9.2 ppm, 1–71 ppm, 1.8–33.7 ppm and 1–4 ppm, respectively (Tables 2 and 3), and are all below those of the averages upper crust (Fig. 7b). As values are moderate, and vary from 0.5 to 11.3 ppm while high values of Au are recorded across the samples (average 849.33 ppb). Most of the samples exhibit positive anomaly in Th, K, La, Ce, Nd, Ni, Rb, and Zr, and negative anormaly in Ba, U, Nb, Ta, Sr, P, Ti, V, Pb and Cu (Fig. 7a and b).

4.5.1. Rare earth elements

Details on REE contents and some related parameters of the studied rocks are summarized in Tables 4 and 5 The total REE and the ratios of LREE to HREE contents are between 32.78 and 501.72 ppm, and 4.72–10.96, respectively. The rocks are characterized by enrichment in LREE (La_N/Sm_N, 4.52–2.29), depletion in HREE (Gd_N/Yb_N, 3.31–1.17), and significant negative Eu anomalies (0.57–0.80). Comparison of the chondrite-normalized distribution of ASU rocks to UCC and Post Archean Australian Shale (PAAS) (Taylor and McLennan, 1985, 1995), show some similarities (Fig. 8). However, the concentrations of the quartzites are lower than those of UCC and PAAS (Fig. 8) while the concentrations of schist and micaschist samples are generally higher than those of these UCC and PAAS (Fig. 8**).** This shows that the studied schistose rocks contain more REE concentrations than those of the quartzites; thus confirming the quartz enrichment in the quartzites. Also, the chondrite normalized La/Yb ratio varies between 7.18 and 20.83, with most rocks samples having contents relatively more abundant than those of UCC and PAAS. Furthermore, the Europium anomaly matches with the depletion in CaO and Na_2O, indicating that it moderately developed in response to plagioclase weathering, where most of the Europium is incorporated. McLennan and Taylor (1991) and Awwiller (1994), supposed that the Europium anomaly in sedimentary rocks is commonly believed to be derived from igneous source rocks.

5. Discussion

5.1. Influence of metamorphism/alteration

The major elements such as Si, Ca, K, and Na and mobility of trace elements such as Cs, Rb, Ba, and Sr of sedimentary rocks can be affected by alteration and metamorphism (Bhatia, 1983; Roser and Korsch, 1986; Bhatia and Crook, 1986; Yang et al., 1998). Consequently, it is essential to examine the scale of metamorphism, alteration and element mobility on the analysed rocks samples before making good inferences with the geochemical data obtained in this study. Several observations prove low degree of metamorphism and alteration in the area, and insignificant extent remobilization of some trace elements. In fact, the rocks of the Atacora Structural Unit reflect a greenschist metamorphic facies

Table 4
REE (ppm), some ratio and main parameters for quartzite samples.

Lithology	Quartzite								
Sample	AD4	AD6	10 CE	12 CE	19 CE	24 CE	25 CE	31 CE	32 CE
La	21.0	12.4	7.5	11.8	7.0	21.5	7.7	16.6	2.3
Ce	38.5	22.1	13.5	21.1	12.9	41.2	12.9	29.3	3.4
Pr	4.99	3.06	1.79	2.76	1.7	4.86	1.79	3.84	0.52
Nd	18.2	11.8	6.6	11.0	6.7	18.2	6.8	14.3	2.0
Sm	3.07	2.20	1.13	2.03	1.16	3.25	1.21	2.31	0.7
Eu	0.69	0.42	0.27	0.48	0.27	0.72	0.28	0.55	0.12
Gd	2.44	1.67	0.97	1.85	1.06	2.83	1.06	2.05	0.88
Tb	0.36	0.23	0.15	0.27	0.15	0.44	0.15	0.3	0.18
Dy	2.06	1.32	0.84	1.45	0.77	2.54	0.88	1.71	0.86
Ho	0.42	0.27	0.16	0.29	0.16	0.53	0.18	0.38	0.18
Er	1.19	0.65	0.42	0.75	0.4	1.59	0.44	1.03	0.42
Tm	0.16	0.09	0.06	0.10	0.06	0.23	0.06	0.15	0.07
Yb	1.12	0.64	0.36	0.70	0.4	1.50	0.42	0.91	0.64
Lu	0.14	0.09	0.05	0.09	0.05	0.22	0.05	0.15	0.09
(La/Yb)N	12.64	13.06	14.05	11.36	11.80	9.66	12.36	12.30	12.64
(Gd/Yb)N	1.76	2.11	2.17	2.13	2.14	1.52	2.04	1.82	1.98
(La/Sm)N	4.30	3.55	4.17	3.66	3.80	4.16	4.00	4.52	4.30
La/Sc	4.20	6.20	1.90	3.93	2.50	3.58	3.85	5.53	3.50
Th/Sc	0.70	0.80	0.33	0.77	0.27	0.82	0.45	0.93	1.3
La/Co	8.08	8.86	5.20	9.08	5.77	4.48	5.50	5.72	4.12
Th/Co	1.35	1.14	0.67	1.77	0.69	1.02	0.64	0.97	0.76
Cr/Th	9.77	12.83	9.77	11.90	8.69	5.58	6.51	3.49	6.01
Th/Cr	0.10	0.08	0.04	0.08	0.05	0.18	0.04	0.08	0.06
Th/U	5.83	5.33	10.00	7.67	4.00	4.45	4.50	7.00	6.20
La/Th	6.00	7.75	7.5	5.13	9.75	4.39	8.56	5.93	1.77
Zr/Sc	20.96	25.10	10.23	22.80	11.1	36.68	17.05	23.4	15.5
Eu/Eu*	0.77	0.67	0.79	0.76	0.74	0.73	0.76	0.73	0.77
ΣLREE	86.45	51.98	30.79	49.17	29.73	89.73	30.68	89.73	66.9
ΣHREE	7.89	4.96	3.01	5.50	3.05	9.88	3.24	9.88	6.68
ΣREE	94.34	56.94	33.8	54.67	32.78	99.61	33.92	99.61	73.58
LREE/HREE	10.96	10.48	10.23	8.94	9.75	9.08	9.47	9.08	10.01

Table 5
REE (ppm), some ratio and main parameters for mica schist and schist samples.

Lithology	Mica schist					Schist		
Samples	AD9	11 CE	15 CE	AD25a	27 CE	18 CE	AD19a	36 CE
La	19.7	27.9	29.9	39.0	22.3	60.8	18.3	92.5
Ce	43.7	54.6	57.5	120.6	21.3	125.4	34.9	167.4
Pr	4.56	6.43	6.77	10.44	4.98	13.75	4.30	27.59
Nd	17.8	25.6	26.0	37.2	17.6	51.3	16.2	122.2
Sm	3.23	5.47	5.57	6.63	3.64	9.46	3.18	25.4
Eu	0.59	1.42	1.42	1.31	0.91	2.29	0.76	5.56
Gd	3.06	6.22	5.97	5.51	3.29	9.73	3.71	23.08
Tb	0.44	0.97	0.97	0.81	0.49	1.66	0.70	3.16
Dy	2.72	5.97	5.49	4.98	2.82	10.38	4.6	17.16
Ho	0.52	1.20	1.14	0.99	0.50	2.27	1.01	2.90
Er	1.65	3.49	3.23	2.91	1.44	6.47	3.12	7.44
Tm	0.21	0.47	0.40	0.42	0.19	0.86	0.41	0.93
Yb	1.43	2.91	2.69	2.99	1.21	5.36	2.55	5.62
Lu	0.20	0.44	0.39	0.46	0.20	0.74	0.36	0.78
(La/Yb)N	9.29	6.46	7.49	8.79	12.43	7.65	4.84	11.10
(Gd/Yb)N	1.73	1.72	1.79	1.49	2.19	1.46	1.17	3.31
(La/Sm)N	3.84	3.21	3.38	3.70	3.85	4.04	3.62	2.29
La/Sc	6.57	2.54	2.99	2.44	1.17	3.80	1.41	3.85
Th/Sc	1.80	0.75	0.87	1.27	0.20	1.02	0.55	0.39
La/Co	3.03	14.68	13.59	2.27	4.96	4.41	8.71	8.98
Th/Co	0.83	4.37	3.95	1.18	0.84	1.18	3.38	0.91
Cr/Th	6.33	0.82	0.79	4.38	39.60	2.94	0.96	2.91
Th/Cr	0.16	1.21	1.27	0.23	1.04	0.34	0.03	0.34
Th/U	3.60	6.92	6.69	8.46	6.33	7.09	5.46	4.70
La/Th	3.65	3.36	3.44	1.92	5.87	3.73	2.58	9.84
Zr/Sc	59.83	16.56	19.40	14.40	5.69	22.89	17.13	15.68
Eu/Eu*	0.67	0.74	0.75	0.66	0.80	0.73	0.68	0.70
ΣLREE	89.58	121.4	127.2	215.2	70.73	263	77.64	440.7
ΣHREE	10.23	21.67	20.28	19.07	10.14	37.47	16.46	61.07
ΣREE	99.81	143.09	147.4	234.25	80.87	300.47	94.1	501.7
LREE/HREE	8.76	5.60	6.27	11.28	6.98	7.02	4.72	7.22

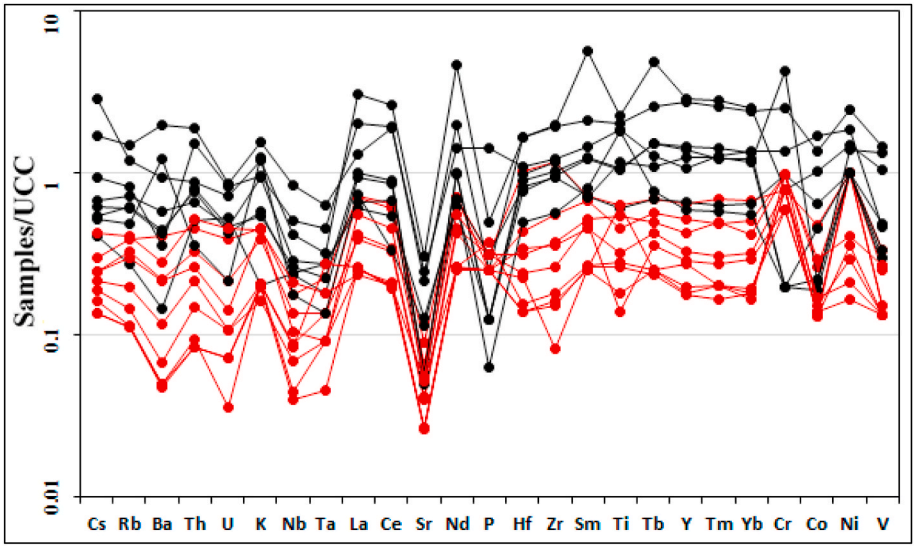


Fig. 7. Spider plots for the ASU metasedimentary rocks showing (a) trace elements plot of the ASU samples normalized against the upper continental crust after Taylor and McLennan (1995), (b) Multiple-elements diagram of the ASU samples normalized against the average crust, after Taylor and McLennan (1985). [In both diagrams, Circle red: quartzites, circle black: schist and micaschist]. (For interpretation of the references to colour in this figure legend, the reader is referred to the Web version of this article.)

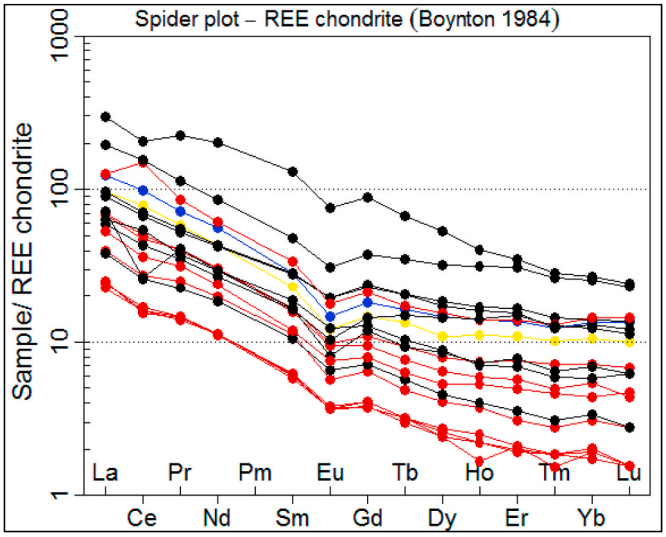


Fig. 8. Chondrite-normalized REE plots for the ASU metasedimentary rocks. [Yellow colour: UCC, blue: PAAS, Circle red: quartzites, circle black: schist and micaschist]. (For interpretation of the references to colour in this figure legend, the reader is referred to the Web version of this article.)

(Affaton et al., 1991; Castaing et al., 1993). The presence epidote and chlorite indicate alteration processes in these rocks According to Shervais et al. (2006), rocks affected by low post-refreshing alteration show $K_2O/P_2O_5 > 1$. The K_2O/P_2O_5 ratios for the analysed samples (Table 2) are greater than 1 ranging between 10.8 and 423. This suggest minor alteration and almost immobility of the major elements.

According to Girty et al. (1996), HFSE and REEs are rarely influenced by post magmatic alteration or metamorphism. This is corroborated by the selected REE and HFSE plot against Zr for the ASU metasedimentary rocks (Fig. 9). The patterns show some levels of scattering and strong linear relationships between Zr and selected trace elements. Particularly, all HFS elements (e.g., Hf, Yb, Nb, Th, and U) illustrate linearly consistent inter-relationships with Zr (Fig. 9) indicating a weak mobility or even non-mobility of these elements. The remaining trace elements (e.g., Tb, Gd, Ce, and Nd) display a low degree of scattering suggesting limited mobility. Their relationships show the consistency and chemical logic of the obtained results. Therefore extensive-scale remobilization, at least for these trace elements was minimal. Hence, it is reasonable to use the geochemical results obtained from the samples in determining the source area weathering characteristics, tectonic setting and provenance (Yang et al., 1998). According to these authors, although it is possible that some LILE are susceptible to be remobilized, the wide extent remobilization of the HFSE and the REEs is limited.Other factors, such as provenance and source area weathering would rather have predominantly contributed in defining the dispersals of these elements.

5.2. *Paleoweathering and metasomatism*

Complex clays (e. g. chlorites, smectite) containing Na, Ca, Mn, Fe and Mg deteriorate easily during weathering comparatively to muscovite and biotite containing K_2O which are stable and unaffected by weathering (Cox et al., 1995). These major elements relationship allow us to deduce the extent of chemical weathering (Nesbitt and Young, 1982, 1984, 1989, 1996). The diagrams of these authors are helpful for deducing the weathering degree of the rocks before being conveyed to their depositional environments. As showed on Al_2O_3–CaO* + Na_2O–K_2O (Fig. 10) ternary diagram, the samples plot along the A-K trend around muscovite-illite closer to high corindon (Al_2O_3) contents (Kaolinite). This suggests that the sediments have experimented an advanced chemical weathering and recorded a K-metasomatism action (i.e, plagioclase albitization and/or illitisation of smectite) from the highly aluminous clays minerals (kaolinite to potassic clays) conversion.

For interpreting the palaeo-weathering history of sediments/metasediments, Nesbitt and Young (1982) and Harnois (1988) suggested the use of the chemical index of alteration (CIA), and of weathering (CIW), respectively, while Fedo et al. (1995) proposed the plagioclase index of alteration (PIA). For calculating the three indices, CaO* (quantity of CaO assimilated in the silicate portion of the rock only but not in carbonate) is used within equations. An indirect method ($CaO^* = CaO - 10/3*P_2O_5$) recommended by McLennan et al. (1993) for determining CaO content has been used in this study.

CIA measures the conversion extent of feldspars to clays minerals. CIA values varying from 0 to 50% point out fresh source areas, whilst values between 50-60% and 60–80% indicate incipient and intermediate weathering, respectively. Values superior or equal to 95%, express a high-degree of weathering at the source area (Nesbitt and Young, 1982). Chemical index of alteration values obtained for quartzites and schistose rocks of ASU vary from 76.11 to 79.65% (average 78.4%) and 74.49–84.20% (average 78.99%), respectively. This suggests that moderate tropical weathering prevails in the source area (Feng et al., 2003; Ejeh et al., 2015; Lang et al., 2018). The obtained values are weakly higher than the PAAS values (70–75%; Taylor and McLennan,

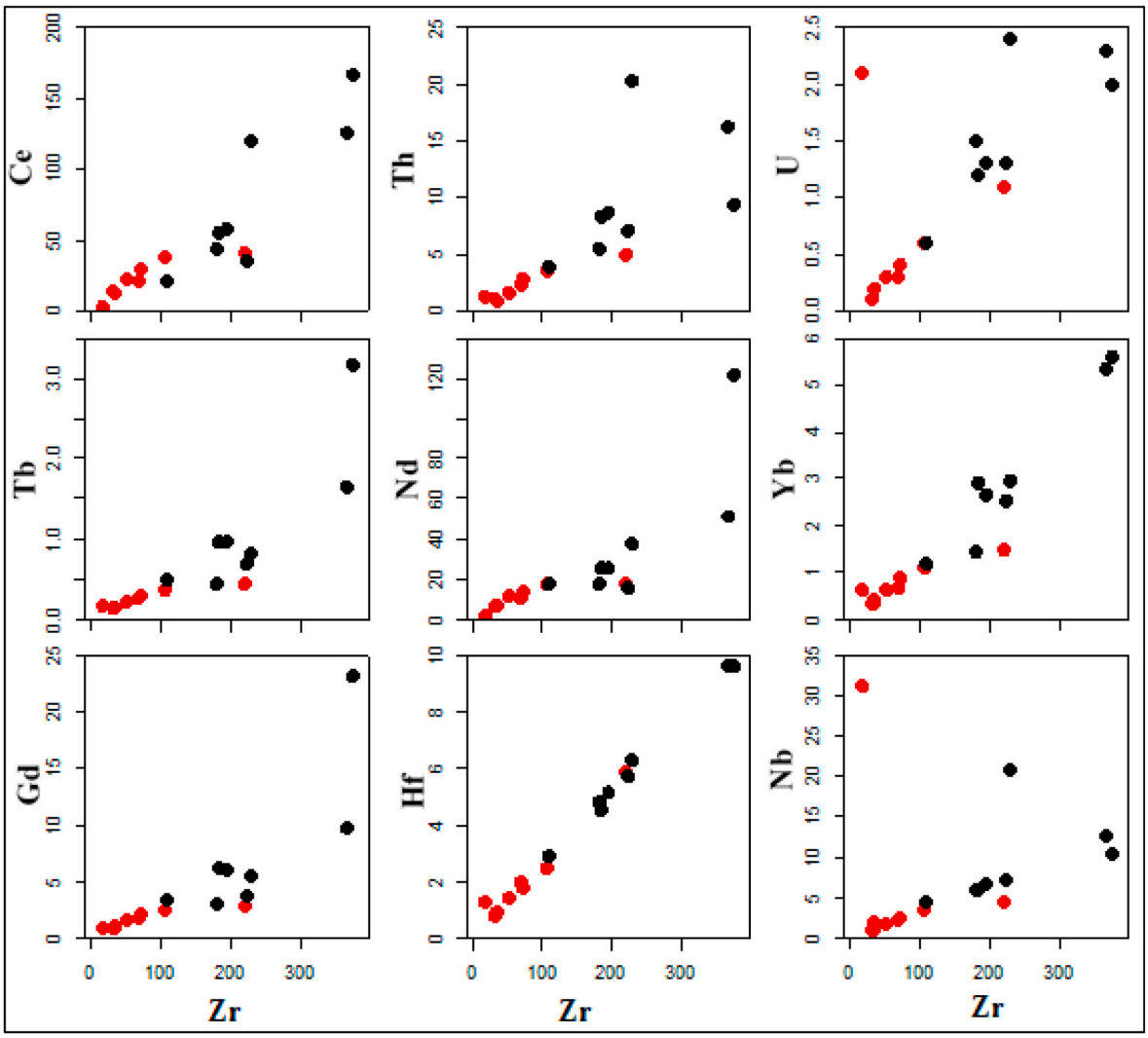


Fig. 9. Multi-plots of Zircon versus selected REE and HFSE for the Atacora Structural Unit. [Red colour: quartzites, black: schist and micaschist]. (For interpretation of the references to colour in this figure legend, the reader is referred to the Web version of this article.)

1985; McLennan et al., 1993). Furthermore, the highest CIA value (CIA = 84.2; sample AD9) could primarily be due to the low values of its K_2O and Na_2O contents or rocks have undergone intensive weathering because of the tropical climate control in the area at the disintegration time of the source rocks.

PIA values ~50% correspond to the unweathered plagioclase values. Values closer to 100% indicate complete plagioclase conversion into others aluminous clay minerals (e.g. chlorite, gibbsite, illite and kaolinite (Fedo et al., 1995). In this study, the high plagioclase index of alteration values (average 96.6%; Tables 2 and 3) of the ASU rocks suggest significant chemical weathering degree at source area. Using CIW criterion, most of the analysed quartzite and schistose rocks show high (>97%) CIW values (Tables 2 and 3) suggestive of advanced weathering at source area (Condie, 1993). In the studied samples, the CIA values are lower than CIW and PIA values because of the elimination of K_2O from the index, hence these rocks would have experienced K-metasomatism.

5.3. Compositional variation and provenance

Using the approach of Roser and Korsch (1988) through major elements discriminant function diagram, Adjo et al. (2021a) stated that the ASU metasedimentary rocks were probably derived from quartzose sedimentary provenance which are mature polycyclic continental sedimentary rocks.

However, compositional variation and sediment degree reworking could be assessed with the Th/Sc versus Zr/Sc plot (McLennan et al., 1993). In this bivariate diagram, sediment samples from igneous differentiation have to accompany the origin-dependent compositional variation tendency while those from recycled sedimentary origin will reassemble towards the zircon addition direction. In this study, the samples plotted along compositional variations trend (Fig. 11a), and not recycled materials and sorting associated with zircon enrichment. The low concentrations of Zircon in most of the rocks (Tables 2 and 3) are in agreement with this diagram. It can be inferred that the protoliths of ASU rocks are mainly derived from igneous rocks (McLennan et al., 1993).

Having constrained principally igneous provenance for the studied ASU rocks, we now attempt to characterize whether their source rocks were predominantly mafic or felsic igneous rocks. The dispersion of transition metals and HFSE rarely undergo the effect of secondary processes, diagenesis and metamorphism. For example, Co, Sc, La, and Th elements are almost immobile during metamorphism and weathering. (Taylor and McLennan, 1985; Wronkiewicz and Condie, 1987; McLennan and Taylor, 1991; Cox et al., 1995). Therefore, the provenance of clastic sedimentary rocks can also be discriminated using HFSE, REEs and some transition elements. While Th and La are more compatible to felsic than mafic igneous rocks, Co and Sc follow the

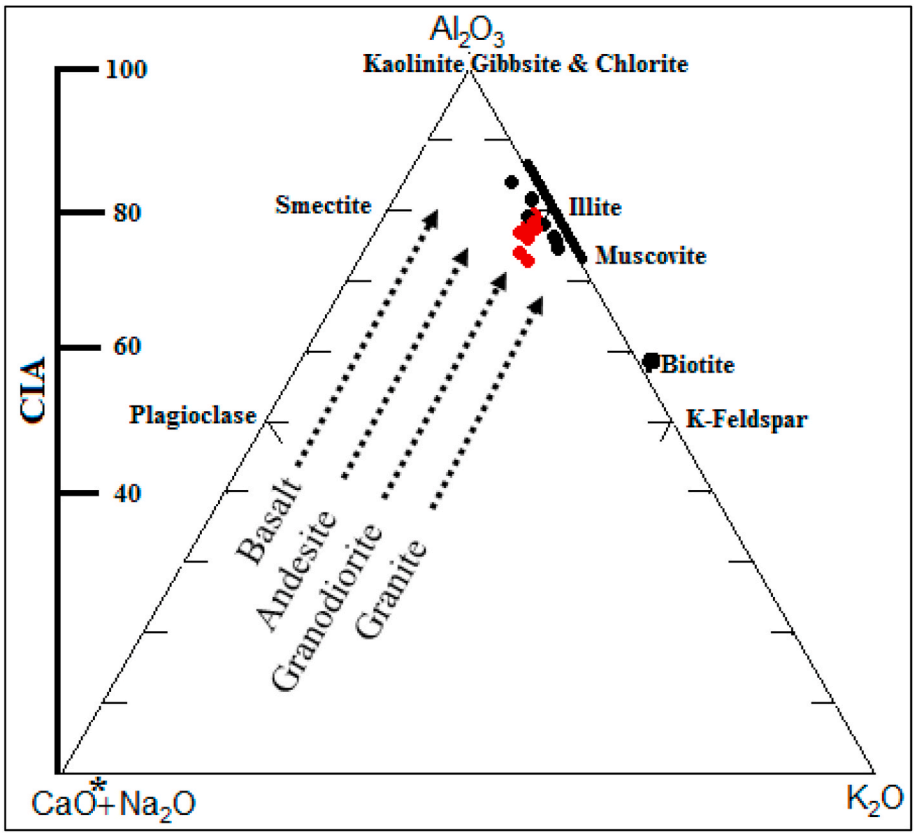


Fig. 10. Paleo weathering discrimination diagrams, after Nesbitt and Young (1982, 1984, 1989, 1996). [Circle red: quartzites, circle black: schist and micaschist]. (For interpretation of the references to colour in this figure legend, the reader is referred to the Web version of this article.)

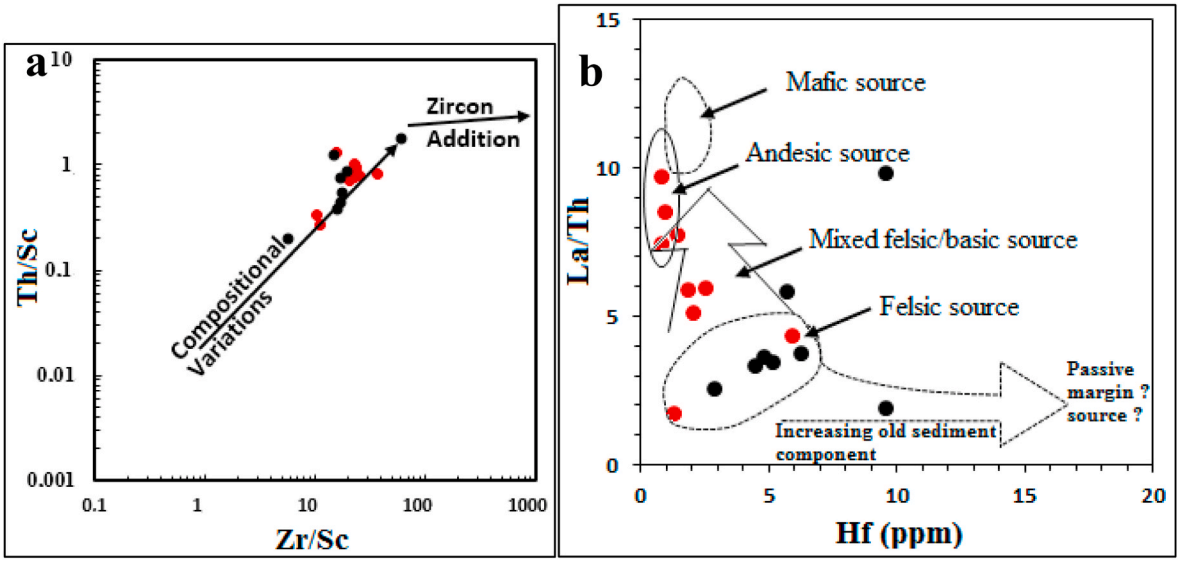


Fig. 11. Composition variation and provenance discrimination diagrams for the ASU metasediments, (a) after McLennan et al. (1993); (b) after Floyd and Leveridge (1987). [Circle red: quartzites, circle black: schist and micaschist]. (For interpretation of the references to colour in this figure legend, the reader is referred to the Web version of this article.)

opposite trend in those rocks. Thus elemental ratios, such as Th/Co, Th/Sc, La/Co, Zr/Sc and La/Sc are useful in the determination of provenance of sedimentary rocks (Taylor and McLennan, 1985; Cullers et al., 1988; McLennan et al., 1993; Cullers, 2002). Some average elemental ratios of the ASU metasedimentary rocks have been compared with other sediments sourced from basic and felsic rocks; these are shown in Table 6. From the comparison, the elemental ratios of the ASU metasedimentary rocks are almost within or close to the average values of the felsic source.

Also, the size and behaviour of the Europium anomaly can be used to infer the source area of metasedimentary rocks because felsic igneous rocks usually hold negative europium anomalies (from REE chondrite-

Table 6
Range of elemental ratios values in the ASU metasedimentary rocks compared to similar ratios values in fractions derived from felsic and mafic rocks (after Cullers et al., 1988; Cullers, 1994, 2000, 2002; Cullers and Podkovyrov, 2000).

Elements ratios	Range of metasediments from ASU [a]			Range of sediments from felsic and mafic sources [b]	
	Quartzites (n = 9)	Schists(n = 3)	Micaschists (n = 5)	Mafic	Felsic
Cr/Th	3.49–12.83	0.96–2.94	0.79–6.33	25–500	4.00–15.0
Th/Cr	0.04–0.18	0.03–0.34	0.16–1.27	0.018–0.046	0.13–2.70
Th/Co	0.64–1.77	0.91–3.38	0.83–4.37	0.04–1.40	0.67–19.4
La/Co	4.12–9.08	4.41–8.98	2.27–14.68	0.14–0.38	1.80–13.8
Th/Sc	0.33–1.30	0.39–1.02	0.75–1.8	0.05–0.22	0.84–20.5
La/Sc	1.90–6.20	1.41–3.85	2.44–6.57	0.43–0.86	2.50–16.3
Eu/Eu*	0.67–0.77	0.66–080	0.67–0.75	0.71–0.95	0.40–0.94

[a] This study.
[b] Cullers et al. (1988). Cullers (1994.2000.2002). Cullers and Podkovyrov (2000). Armstrong-Altrin (2009).

normalized plot patterns) while igneous mafic rocks show no or little europium anomaly (Taylor and McLennan, 1985; Cullers, 2000, 2002). The negative europium anomalies ranging from 0.66 to 0.80 in the studied rocks (Tables 5 and 6) would suggest felsic materials (Cullers et al., 1988; Cullers and Podkovyrov, 2000). Thus, it indicates that the precursors of the studied rocks were extracted from magmatic materials (Taylor and McLennan, 1985). By using the approach of Rudnick (1992), the negative patterns of Europium anomalies on the REE diagrams (Fig. 8) support felsic source. This is further reinforced by the enrichment in LREE relative to HREE, which according to Wang et al. (2016) symbolizes felsic sources for the sediments. Conversely, the Eu/Eu* range, overlaps those of sediments from both felsic and mafic rock sources (Table 6) indicating mixed felsic and mafic sources. All the samples showed negative Europium anomalies, an enrichment in LREE and fractionated HREE patterns (Fig. 8). These characteristics, notably the negative Europium anomalies point to a differentiated photoliths (McLennan et al., 1993; Asiedu et al., 2000). It is known that siliciclastic rocks with Cr/Th values of between 2.5 and 17.5 as well as Eu/Eu* values varying from 0.48 to 0.78, are frequently from felsic sources (Cullers, 1994). Thus, all Eu/Eu* as well average Cr/Th values (Table 6) for the studied rocks fall within the felsic source domain.

On the Hf against La/Th plot (Fig. 11b) which can also discriminate the nature of source rocks and different arc constituents (Floyd and Leveridge, 1987), the studied rocks are deduced to have originated from felsic sources with some involvement from mixed felsic and mafic provenance. In fact, mainly the schistose rocks and a quartzite (24 CE) samples have high Hf values (4.5–9.6 ppm) and low La/Th contents (1.92–4.39) compared to the other quartzite samples; this suggests that most of sediments originated from felsic rock sources with some implications from the recycling of ancient sediment. Three quartzite samples have low Hf concentrations (1.4–2.5 ppm) and slightly high La/Th ratios (5.13–9.75) indicating a combination of mafic and felsic source areas, and probably implicating subduction of oceanic crust on continental margin (Floyd et al., 1989).

One of the sample (36 CE, schist) plotting outside these fields may probably be a recycled sediment (Fig. 11b). It contains slightly high La/Th and Hf values (9.84 and 9.6 ppm, respectively). This high Hf concentration can imply high zircon content in the sediment, while high La/Th value could be related to low Thorium concentration in the sediment.

Nevertheless, most of the ASU samples with Hf contents (2–6.3 ppm) and La/Th values (1.92–5.13) are mostly felsic in composition since these averages are similar to those of Floyd and Leveridge (1987) who demonstrated that, felsic source arcs show constant or low (less than 5) La/Th values and Hf contents range from 3 to 7 ppm.

From the above discrimination diagrams, trace element ratios, and other immobile elements ratio diagrams, it is reasonable to propose that the protolith of the studied ASU quartzites, mica schists and chlorite-sericite-quartz schists were largely sourced from felsic rocks with involvements from mixed mafic and felsic regions beside ancient recycled components. The felsic material could also have evolved from the fractionation of a mafic melt. This interpretation of combined provenance is also supported by detrital zircon which yielded three different ages (993–597 Ma (Neoproterozoic), 1598–1006 Ma (Mesoproterozoic) and (2225–1704 Ma (Paleoproterozoic) in the schists and quartzites of the ASU (Ganade et al., 2016).

From the above deduction, it appears that the quartzite and schist rocks of the ASU mainly derived from felsic sources (probably granitoids) with mafic source rocks (basalt) contributions.

5.4. Source area location

Having deduced a principally granitic materials with involvements from mafic regions derivation for the precursors of the studied ASU metasediments, it seems useful to discriminate these source regions. The metasediments of ASU are interpreted as metamorphic and tectonic lateral equivalents of the sediments of Bombouaka Group of Volta Basin. (Affaton, 1990; Affaton et al., 1991). Thus, the Bombouaka Group sedimentary rocks and the ASU metasedimentary rocks might have a common source area or at least a felsic rocks source. Ganade et al. (2016) support this inference using compatible detrital zircon signatures between the ASU and Volta Basin rocks. Also, (a) given that the Volta basin thrusts to the East of the WAC while the ASU is thrusted by the

Table 7
Comparison of some trace elements ratios of the ASU metasedimentary rocks to those of the Boumbouaka Group and Birimian metasedimentary rocks.

Elements ratios	Range of metasediments from ASU [a]			Range of Neoproterozoic Bombouaka sandstones [b]	Range of Paleoproterozoic Birimian sedimentary rocks [c]
	Quartzites	Schists	Micaschists		
Th/Cr	0.04–0.18	0.03–0.34	0.16–1.27	0.05–0.44	0.026–0.061
Th/Co	0.64–1.77	0.91–3.38	0.83–4.37	0.52–8.26	0.16–0.35
La/Co	4.12–9.08	4.41–8.98	2.27–14.68	1.46–28.1	0.33–2.33
La/Th	1.77–9.75	2.58–9.84	1.92–5.87	1.93–14.4	2.08–8.87
Th/Sc	0.33–1.30	0.39–1.02	0.75–1.80	0.73–6.24	0.09–0.47
La/Sc	1.90–6.20	1.41–3.85	2.44–6.57	2.07–28.1	0.38–2.71
Eu/Eu*	0.67–0.77	0.66–080	0.57–0.75	0.50–0.71	0.71–0.97

[a] This study.
[b] Anani et al., 2017.
[c] Asiedu et al., 2004 & 2017.

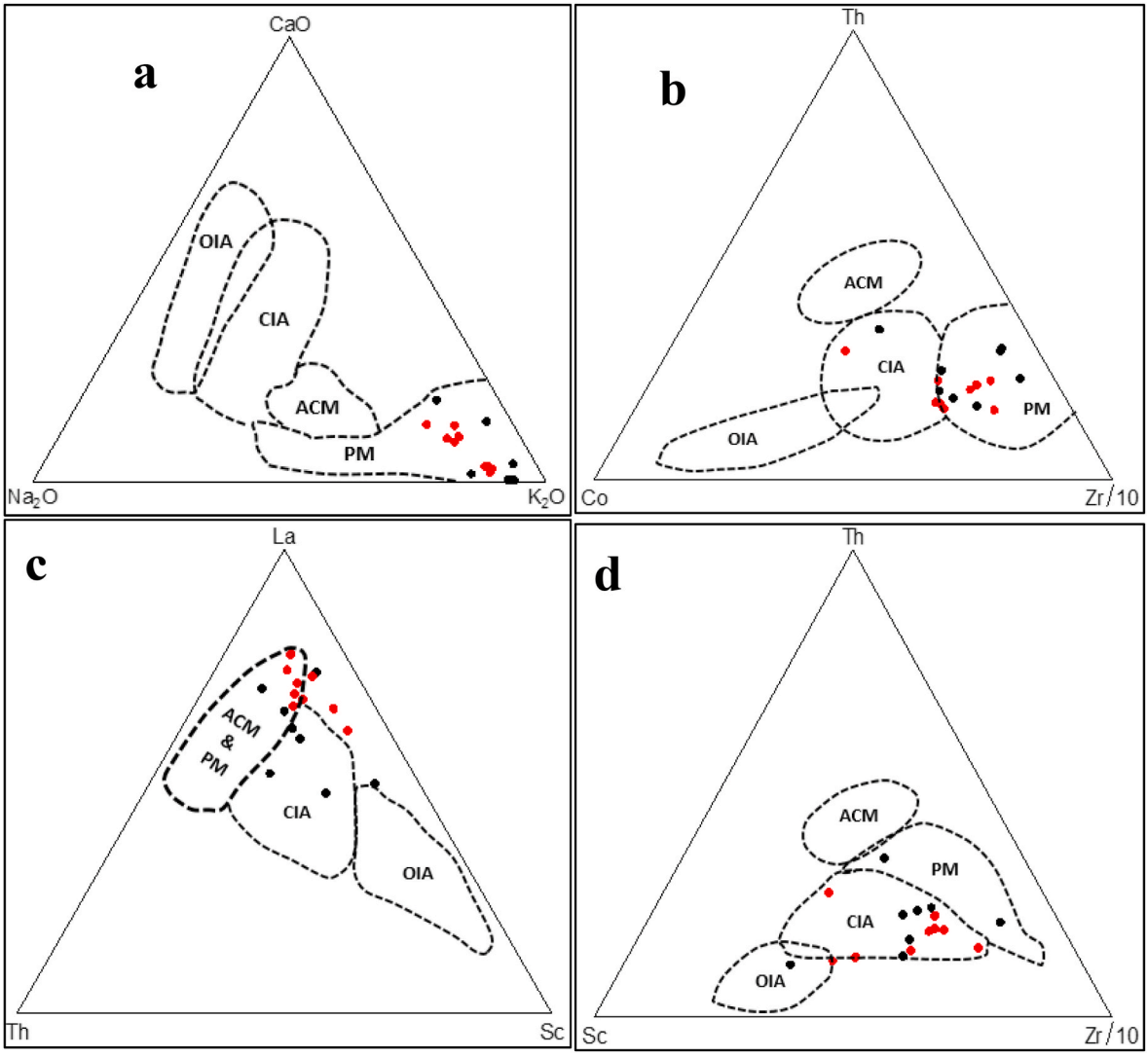


Fig. 12. Plot of the ASU metasediments data on various diagrams using major oxides and trace elements contents such as **(a)** CaO–Na_2O–K_2O ternary diagram after Toulkeridis et al. (1999); **(b)** Th–Co–Zr/10 ternary diagram**; (c)** La–Th-Sc ternary diagram and **(d)** Th-Sc-Zr/10 ternary diagram after Bhatia and Crook (1986). [Circle red: quartzites; circle black: schist and micaschist]. (For interpretation of the references to colour in this figure legend, the reader is referred to the Web version of this article.)

basement nappes, and (b) that the studied metasedimentary rocks yielded Pan-African age (662–579 Ma; Attoh et al., 1997; Ganade et al., 2016), the only older rocks displayed in West Africa around the basin and ASU and able to provide detritus to the Bombouaka Group/ASU are Paleoproterozoic rocks (2000–2200 Ma; Abouchami et al., 1990; Leube et al., 1990; Taylor et al., 1992; Davis et al., 1994), and migmatitic and granitic gneisses and associated rocks of the basement nappes (basement rocks).

To investigate these hypothesis a comparison between some sensitive trace elements ratios of the studied ASU rocks and those of the Boumbouaka Group (Neoproterozoic) and Birimian metasedimentary rocks were performed (Table 7) since the high concentrations of least fractionated REEs, Sc and Th in the sediments are linked to that of their source (McLennan et al., 1980). The geochemical proprieties of the studied ASU rocks are analogous to geochemical particularities of the Bombouaka sandstones documented by Anani et al. (2017). Their Th/Cr, La/Co, La/Sc, Th/Co, Th/Sc ratios and europium anomalies values are similar (Table 7). Further, both show Na_2O and CaO depletion, and K_2O-rich concentrations higher than Upper Continental Crustal values. These various geochemical comparisons suggest that the ASU metasedimentary rocks and the sedimentary rocks of the Bombouaka Group can have a same source area and igneous provenance. This understanding is enhanced by similar detrital zircon ages yielded in both the sedimentary rocks of Bombouaka Group and the ASU metasedimentary rocks with 993–2225 Ma (ASU; Ganade et al., 2016) and 1100–2200 Ma (Bombouaka Group; Kalsbeek et al., 2008) which overlap that of the flanking Birimian Paleoproterozoic basement (2000–2200 Ma).

Contrary to the geochemical similarities noticed between the Bombouaka Group sedimentary rocks and those analysed, the geochemical characteristics of the ASU rocks are expressively dissimilar to those of the Birimian metasedimentary rocks reported by Asiedu et al. (2004 & 2017). For example, the Eu/Eu* of these Birimian metasedimentary rocks are larger than those of ASU metasedimentary rocks. Likewise, the Th/Sc, La/Sc, La/Co, Th/Co and Th/Cr values of the studied ASU rocks are considerably higher than those of the Birimian metasedimentary rocks documented by Asiedu and his collaborators in 2004 and 2017. Consequently, the Birimian rocks, susceptible to be exposed for erosion and fed the Volta basin (indirectly the ASU) with sediments, are improbable to be the main source of the ASU metasedimentary rocks. Hence, the proximal granitoids from the basement nappes are the most likely candidates. Furthermore, the rocks of the Bombouaka Group and those of Togo Structural Unit, all lateral

Table 8
Sensitive parameters discriminator of tectonic setting (Bhatia and Crook, 1986).

Tectonic setting		La	Ce	ΣREE	La/Yb	(La/Yb)N	ΣLREE/ΣHREE	Eu/Eu*
CIA[a]		27 ± 4.5	59 ± 8.2	146 ± 20	11 ± 3.6	7.5 ± 2.5	7.7 ± 1.7	0.79 ± 0.13
OIA[a]		8 ± 1.7	19 ± 3.7	58 ± 10	4.2 ± 1.3	4.2 ± 1.3	3.8 ± 0.9	1.01 ± 0.11
PM[a]		39	85	210	15.9	10.8	8.5	0.56
ACM[a]		37	78	186	12.5	8.5	9.1	0.6
Quartzites[b]	04 CE	21	38.5	94.34	18.75	12.64	10.96	0.77
	06 CE	12.4	22.1	56.94	19.38	13.06	10.48	0.67
	10 CE	7.8	13.5	33.8	19.5	14.05	10.23	0.79
	12 CE	11.8	21.1	54.67	16.86	11.36	8.94	0.76
	19 CE	7.5	12.4	32.78	20.83	11.80	9.75	0.74
	24 CE	21.5	41.2	99.61	14.33	9.66	9.08	0.73
	25 CE	7.7	12.9	33.92	18.33	12.36	9.47	0.76
	31 CE	16.6	29.3	99.61	18.24	12.30	9.08	0.73
	32 CE	7.0	3.4	73.58	10.94	12.64	10.01	0.77
Micaschists[b]	AD9	19.7	43.7	99.81	13.78	9.29	8.76	0.57
	11 CE	27.9	54.6	143.09	9.59	6.46	5.60	0.74
	15 CE	29.9	57.5	147.44	11.12	7.49	6.27	0.75
	AD25a	39	120.6	234.25	13.04	8.79	11.28	0.73
	27 CE	22.3	21.3	80.87	18.43	12.43	6.98	0.68
Schists[b]	18 CE	60.8	125.4	300.47	11.34	7.65	7.02	0.66
	AD19a	18.3	34.9	94.1	7.18	4.84	4.72	0.80
	36 CE	92.5	167.4	501.72	16.46	11.10	7.22	0.70

[a] Sandstones from different tectonic setting (Bhatia, 1985).
[b] This study.

equivalent of ASU rocks, revealed zircon ages of 1000–1300 Ma (Kalsbeek et al., 2008). This age tranche are characteristic of rocks sourced from outside the WAC, likely from the Amazonian Craton (Kalsbeek et al., 2008). Considering the parallel ages of deposition and the lateral coherence between the ASU, TSU and sequences of Bombouaka, the protolith of the ASU metasedimentary rocks might also source from the Amazonian Craton. The rocks of Bombouaka Group and those of the ASU yielded detrital zircon ages analogous with the adjoining WAC which is similar to that of the Martinópole in North-east Brazil situated within the Amazonian Craton, referred as a perfect equivalence of the ASU Ganade et al. (2016).

In sum, considering the above geochemical analysis results, previous data of Zircon ages and various correlations between the units, we propose that the ASU metasedimentary rocks resulted from sedimentary rocks which might be originated from the migmatitic and granitic gneissic rocks of the basement nappes and/or rocks from the Amazonian Craton.

5.5. Tectonic setting

According to Verma and Armstrong-Altrin (2016), siliciclastic sediments can be classified considering the tectonic environment of their source rocks since the composition of the sediemnts is predominated by composition of the provenance area which is furthermore controlled by the tectonic context. This contribution attempts to constrain the tectonic context of the analysed ASU metasedimentary rocks using the approach of Bhatia and Crook (1986) and Toulkeridis et al. (1999).

On the calc-alkaline plot ($CaO–Na_2O–K_2O$) proposed by Toulkeridis et al. (1999), all the studied samples shown characteristic of being within the passive margin (PM) field (Fig. 12a). Moreover, based on some characteristics, including constancy and uniformity of some elements (La, Sc, Co, Th and Zr) of sediments during the post depositional process, Bhatia and Crook (1986) suggested several types of diagrams to discriminate tectonic regime. In Fig. 12b showing the ternary model of Th–Co–Zr/10, the analysed rocks predominantly plot within the PM field, but two samples plotted in the CIA field. On the Th–La-Sc diagram the rocks plotted largely within the continental margin field (Fig. 12c), while six samples are situated close to it but in the CIA field. As showed on the ternary diagram of Th-Sc-Zr/10 (Fig. 12d), almost all of the ASU rocks plotted within or inside the vicinity of the CIA area, with two of them within the PM field and one plot in OIA.

Furthermore, the most sensitive discriminators of the tectonic context (Bhatia and Crook, 1986), Sc, Hf, Th, Zr, and ΣREE concentration, Eu/Eu* and Zr/Hf ratio, with means of 10.67 ppm, 7.63 ppm, 5.03 ppm, 191.93 ppm, 158.94 ppm, 0.73 and 37.9, respectively, are similar to those recorded in the sedimentary rocks of continental island arc (Table 8). Inversely, other indicators, such as Zn, Nd, La, Ce, V, Co Nb, Th/U, Rb/Sr and La/Y with averages of 10.5 ppm, 31.09 ppm, 31.43 ppm, 62.36 ppm, 32.92 ppm, 5.72 ppm, 7.13 ppm, 6.04, 1.83 and 1.39, respectively are close to those documented in sedimentary rocks of passive margin environment (Tables 4, 5 and 8; Bhatia and Crook, 1986). In addition, Zr/Th (28.93), La/Yb (14.18) and La/Yb normalized (9.56) approximate the two different tectonic settings. In sum, the above different discrimination parameters and diagrams indicate features of both PM and CIA tectonic setting for the ASU metasedimentary rocks, but with a dominance of passive margin materials in the source. Eventually, the rocks that plotted in CIA field, are built on either 'thin continental margin or on well-developed continental crust' with a source of a "dissected magmatic arc-recycled orogen" (Bhatia, 1983; Bhatia and Crook, 1986). However, the sample which plotted in OIA is probably due to a contaminant introduced during the preparation of samples.

Previous works (Affaton et al., 1980; Trompette, 1994; Ganade et al., 2016) in the Volta Basin and Atacora Structural Unit have interpreted the tectonic context of the regions as passive margin deposits similarly to those of Amedjoe et al. (2018) that concluded passive margin settings for Volta Basin sediments with painting of continental island arc settings materials. Though the geochemistry of sediments does not constrain age of CIA sediments, it seems that, mature CIA basement residues from cropping rocks at the Passive Margin location may have played on the sediments chemistry (Amedjoe et al., 2018). Consequently, the tectonic context metasedimentary rocks of the Atacora Structural Unit point out characteristics of both Continental Island arc and passive margin with predominant of passive margin materials.

6. Conclusion

Petrography and geochemical studies were performed to constrain the paleoweathering, tectonic setting and provenance of quartzites, mica schists and chlorite-sericite-quartz schist succession of the Atacora structural unit within the Natitingou area. From the obtained data, the following four key conclusions emerge:

Firstly, petrography characteristics show that the studied rocks are

quartz-rich with a moderate proportion of K-feldspar, which is also supported by geochemical analysis. Textural characteristic classify them as sublitharenite/quartzarenite while the major elements data classify quartzite as subarkose/sublitharenite and schistose rocks as arkoses. The CIA, PIA and CIW indices indicated that the metasedimentary rocks of ASU were sourced from a moderately to relatively high degree weathered and humid paleoclimate in source area. Also, the high constituent maturity and large range of CIA and CIW values indicate that the rocks experienced a long-distance transport.

Secondly, the REE patterns of chondrite-normalized, and Th/Sc, La/Th, Th/Co, Cr/Th and Zr/Sc) ratios suggest that the rocks are composed predominantly of sedimentary materials which originated mainly from felsic materials with minor basic contributions. The chondrite-normalized REE patterns, with substantial negative Europium anomaly, LREE enrichment and almost flat HREEs indicate Upper Continental Crustal materials for the studied metasediments.

Thirdly, the ASU metasedimentary rocks have divergent geochemical features from the metasedimentary rocks of the basement Birimian, with higher Th/Sc, La/Co, Th/Cr, Th/Co, La/Sc ratios and small negative Eu anomalies. In contrast, their geochemistry are comparable to the Bombouaka Group sedimentary rocks, thus indicating that they were sourced from identical areas, possibly the migmatitic and granitic gneisses of the Dahomeyide basement or rocks exposed within the Amazonian craton.

Fourthly, several tectonic setting discrimination models and sensitive parameters show dominant characteristics of passive margin tectonic setting with mixed of continental island arc tectonic environment.

Declaration of competing interest

The authors declare there is no conflict of interests.

Acknowledgments

This study is funded by the African Union through a PhD Scholarship scheme to the first author at Pan African University, Life and Earth Science Institute (PAULESI), Ibadan University, Ibadan, Nigeria. We thank all anonymous reviews for their comments and suggestions which significantly enriched our manuscript.

References

Abouchami, W., Boher, M., Michard, A., Albarede, F., 1990. A major 2.1 Ga old event of mafic magmatism in West Africa: an early stage of crustal accretion. J. Geophys. Res. 95, 17605–17629.

Adjo, F.B., 2021. Geological Studies and Metallogenesis of Gold Mineralisation in the Natitingou Area, Atacora Structural Unit, Northwestern Benin Republic. Thesis dissertation, University of Ibadan, p. 292.

Adjo, F.B., Adissin Glodji, L., Bolarinwa, A.T., Nude, P.M., Anagonou, B., 2021a. Geochemistry of gold-bearing metamorphic rocks of the Natitingou area, Atacora structural unit, Northwestern Bénin (West Africa): implications for Au genesis. Geochemistry 81 (2). https://doi.org/10.1016/j.chemer.2021.125739, 125739.

Adjo, F.B., Bolarinwa, A.T., Adissin Glodji, L., Nguimatsia Dongmo, F.W., Olajide-Kayode, J.O., 2019. A review of the current state of knowledge on gold mineralisation in Benin Republic, West Africa. B. Appl. Earth Sci. 128 (1), 2–14.

Adjo, F.B., Bolarinwa, A.T., Adissin Glodji, L., Nude, P.M., Anagonou, B., Olajide-Kayode, J.O., 2021b. Petrographic, geochemical and structural characteristics of gold-bearing metasedimentary rocks from the Atacora structural unit, northwestern Bénin republic. Arab J Geosci 14, 734.

Affaton, P., 1990. Le bassin des Volta (Afrique de l'Ouest): une marge passive, d'âge protérozoïque supérieur, tectonisée au Panafricain (600 ± 50 Ma). Thèse de doctorat d'Etat, Université Aix-Marseilles III, p. 462 (Unpublished doctoral dissertation).

Affaton, P., Rahaman, M.A., Trompette, R., Sougy, J., 1991. The dahomeyide orogen: tectonothermal evolution and relationships with the Volta basin. In: Dallmeyer, R.D., Lécorché, J.P. (Eds.), The West African Orogens and Circum-Atlantic Correlatives. Springer-Verlag, Berlin, pp. 107–122.

Affaton, P., Sougy, J., Trompette, R., 1980. The tectono-stratigraphic relationships between the upper precambrian and lower paleozoic Volta basin and the pan-african dahomeyide orogenic belt (West Africa). Am. J. Sci. 280, 224–248.

Agbossoumondé, Y., Ménot, R.P., Paquette, J.L., Guillot, S., Yéssoufou, S., Perrache, C., 2007. Petrological and geochronological constraints on the origin of the palimé–amlamé granitoids (south Togo, West Africa): a segment of the west african craton paleoproterozoic margin reactivated during the pan-african collision. Gondwana Res. 12, 476–488.

Aidoo, F., Zhang, S.-B., Sun, F.-Y., Liang, T., Nude, P.M., 2020. New insight into the dahomeyide belt of southeastern Ghana, West Africa: evidence of arc-continental collision and neoarchaean crustal reworking. Precambrian Res. https://doi.org/10.1016/j.precamres.2020.105836.

Anani, C.Y., Bonsu, S., Kwayisia, D., Asiedu, D.K., 2019. Geochemistry and provenance of Neoproterozoic metasedimentary rocks from the Togo structural unit, Southeastern Ghana. J. Afr. Earth Sci. 153, 208–218.

Anani, C.Y., Mahamuda, A., Kwayisi1, D., Asiedu, D.K., 2017. Provenance of sandstones from the neoproterozoic Bombouaka group of the Volta basin, northeastern Ghana. Arab J Geosci 10, 465.

Amedjoe, C.G., Gawu, S.K.Y., Ali, B., Aseidu, D.K., Nude, P.M., 2018. Geochemical compositions of neoproterozoic to lower palaeozoic (?) shales and siltstones in the Volta basin (Ghana): constraints on provenance and tectonic setting. Sediment. Geol. 368, 114–131.

Armstrong-Altrin, J.S., 2009. Provenance of sands from cazones, acapulco and bahía kino beaches, Mexico. Rev. Mex. Ciencias Geol. 26 (3), 764–782.

Asiedu, D.K., Asong, S., Atta-Peters, D., Sakyi, P.A., Su, B.X., Dampare, S.B., Anani, C.Y., 2017. Geochemical and Nd-isotopic compositions of juvenile-type Paleoproterozoic Birimian sedimentary rocks from southeastern West African Craton (Ghana): constraints on provenance and tectonic setting. Precambrian Res. 300, 40–52.

Asiedu, D.K., Dampare, S.B., Sakyi, P.A., Banoeng-Yakubo, B., Osae, S., Nyarko, B.J.B., Manu, J., 2004. Geochemistry of Paleoproterozoic metasedimentary rocks from the Birim diamondiferous field, southern Ghana: implications for provenance and crustal evolution at the Archean–Proterozoic boundary. Geochem. J. 38, 215–228.

Asiedu, D.K., Suzuki, S., Nogami, K., Shibata, T., 2000. Geochemistry of lower cretaceous sediments, inner zone of southwest Japan: constraints on provenance and tectonic environment. Geochem. J. 34, 155–173.

Attoh, K., Dallmeyer, R.D., Affaton, P., 1997. Chronology of nappe assembly in the Pan-African Dahomeyide orogen, West Africa: evidence from 4°Ar/39Ar mineral ages. Precambrian Res. 82, 153–171.

Attoh, K., Nude, P.M., 2008. Tectonic significance of carbonatite and ultrahigh- pressure rocks in the Pan– African Dahomeyide suture zone, southeastern Ghana. From. In: Ennih, N., Leiégeois, J.P. (Eds.), The Boundaries of the West African Craton, vol. 297. Geol. Soc. London Spec. Pub., pp. 217–231

Awwiller, D.N., 1994. Geochronology and mass transfer in Gulf Coast mudrocks (south-central Texas, USA): Rb-Sr, Sm-Nd and REE systematics. Chem. Geol. 116, 61–84.

Bessoles, B., Trompette, R., 1980. Géologie de l'Afrique: La chaine panafricaine: «zone mobile d'Afrique centrale (partie sud) et zone mobile soudanaise ». B.R.G.M., Orleans, France, 397p, (Unpublished report).

Bhatia, M.R., 1983. Plate tectonics and geochemical composition of sandstones. J. of Geology 91 (6), 611–627.

Bhatia, M.R., 1985. Rare earth element geochemistry of Australian Paleozoic graywackes and mudrocks: provenance and tectonic control. Sediment. Geol. 45 (1–2), 97–113.

Bhatia, M.R., Crook, K.A., 1986. Trace element characteristics of graywackes and tectonic setting discrimination of sedimentary basins. Contrib. Mineral. Petrol. 92 (2), 181–193.

Caby, R., 1989. Precambrian terranes of Benin-Nigeria and northeast Brazil and the late proterozoic south atlantic fit. Geol. Soc. Am. Spec. Pap. 230, 145–158.

Castaing, C., Triboulet, C., Feybesse, J.L., Chèvremont, P., 1993. Tectonometamorphic evolution of the Ghana, Togo and Benin in the light of the Pan-African/Brasiliano orogeny. Tectonophysics 218, 323–342.

Condie, K.C., 1993. Chemical composition and evolution of the upper continental crust: contrasting results from surface samples and shales. Chem. Geol. 104, 1–37.

Condie, K.C., 1991. Another look at rare earth elements in shales. Geochem. Cosmochim. Acta 55, 2527–2531.

Cox, R., Lowe, D.R., 1995. A conceptual review of regional-scale controls on the composition of clastic sediment and the co-evolution of continental blocks and their sediment cover. J. Sediment. Res. A65 (1), 1–12.

Cox, R., Lowe, D.R., Cullers, R.L., 1995. The influence of sediment recycling and basement composition on evolution of mudrock chemistry in the south-western United States. Geochem. Cosmochim. Acta 59, 2919–2940.

Crook, K.A.W., 1974. Lithogenesis and Geotectonics: the Significance of Compositional Variation in Flysch Arenites (Graywackes), vol. 19. Society of Economic Paleontologists and Mineralogists, Special Publication, pp. 304–310.

Cullers, R.L., 1994. The controls on the major and trace element variation of shales, siltstones, and sandstones of Pennsylvanian-Permian age from uplifted continental blocks in Colorado to platform sediment in Kansas, USA. Geochem. Cosmochim. Acta 58 (22), 4955–4972.

Cullers, R.L., 2000. The geochemistry of shales, siltstones and sandstones of Pennsylvanian Permian age, Colorado, USA: implications for provenance and metamorphic studies. Lithos 51, 181–203.

Cullers, R.L., 2002. The source and origin of terrigenous sedimentary rocks in the Mesoproterozoic Ui group, south-eastern Russia. Precambrian Res. 117, 157–183.

Cullers, R.L., Basu, A., Suttner, L.J., 1988. Geochemical signature of provenance in sand size material in soils and stream sediments near the Tobacco Root batholith, Montana, USA. Chem. Geol. 70 (4), 335–348.

Cullers, R.L., Podkovyrov, V.N., 2000. Geochemistry of the Mesoproterozoic Lakhanda shales in southeastern Yakutia, Russia: implications for mineralogical and provenance control, and recycling. Precambrian Res. 104 (1–2), 77–93.

Davis, D.W., Hirdes, W., Schaltegger, U., Nunoo, E.A., 1994. U-Pb age constraints on deposition and provenance of Birimian and gold bearing Tarkwaian sediments in Ghana, West Africa. Precambrian Res. 67, 89–107.

Deynoux, M., Affaton, P., Trompette, R., Villeneuve, M., 2006. Pan-African tectonic evolution and glacial events registered in Neoproterozozoic to Cambrian cratonic and foreland basins of West Africa. J. Afr. Earth Sci. 46, 397–426.
Ejeh, O.I., Akpoborie, I.A., Etobro, A.I., 2015. Heavy minerals and geochemical characteristics of sandstones as indices of provenance and source area tectonics of the Ogwashi-Asaba Formation, Niger Delta Basin. Open J. Geol. 5, 562, 08.
Fedo, C.M., Eriksson, K.A., Krogstad, E.J., 1996. Geochemistry of shales from the Archean (3.0 Ga) Buhwa Greenstone Belt, Zimbabwe: implications for provenance and source area weathering. Geochem. Cosmochim. Acta 60, 1751–1763.
Fedo, C.M., Nesbitt, H.W., Young, G.M., 1995. Unravelling the effects of potassium metasomatism in sedimentary rocks and paleosols, with implications for paleoweathering conditions and provenance. Geology 23, 921–923.
Feng, L.J., Chu, X.L., Zhang, Q.R., Zhang, T.G., 2003. CIA (chemical index of alteration) and its application in the Neoproterozoic clastic rocks. Earth Sci. Front. 10, 539–544.
Floyd, P.A., Leveridge, B.E., 1987. Tectonic environment of the Devonian Gramscatho basin, south Cornwall: framework mode and geochemical evidence from turbiditic sandstones. J. Geol. Soc. 144 (4), 531–542.
Floyd, P.A., Winchester, J.A., Park, R.G., 1989. Geochemistry and tectonic setting of lewisian clastic metasediments from the early proterozoic loch maree group of gairloch, NW scotland. Precambrian Res. 45 (1–3), 203–214.
Folk, R.L., 1980. Petrology of Sedimentary Rocks. Hemphill publishing Co, Austin, Texas, p. 182.
Gabo, J.A.S., Dimalanta, C.B., Asio, M.G.S., Queano, K.L., Yumul Jr., G.P., Imai, A., 2009. Geology and geochemistry of the clastic sequences from Northwestern Panay (Philippines): implications for provenance and geotectonic setting. Tectonophysics 479 (1–2), 111–119. https://doi:10.1016/j.tecto.2009.02.004.
Ganade, C.E., Cordani, U.G., Agbossoumounde, Y., Caby, R., Basei, M.A.S., Weinberg, R. F., Sato, K., 2016. Tightening-up NE Brazil and NW Africa connections: new U-Pb/Lu-Hf zircon data of a complete plate tectonic cycle in the Dahomey belt of the West Gondwana Orogen in Togo and Benin. Precambrian Res. 276, 24–42.
Girty, G.H., Ridge, D.L., Knaack, C., Johnson, D., Al-Riyami, R.K., 1996. Provenance and depositional setting of Paleozoic chert and argillite, Sierra Nevada, California. J. Sediment. Res. 66 (1), 107–118.
Harnois, L., 1988. The CIW index: a new chemical index of weathering. Sediment. Geol. 55, 319–322.
Hu, X.M., Garzanti, E., An, W., 2015. Provenance and drainage system of the Early Cretaceous volcanic detritus in the Himalaya as constrained by detrital zircon geochronology. J. Palaeogeogr. 4, 85–98.
Kalsbeek, F., Affaton, P., Ekwuemec, B., Frei, R., Thrane, K., 2012. Geochronology of granitoid and metasedimentary rocks from Togo and Benin, West Africa: comparisons with NE Brazil. Precambrian Research 196– 197, 218–233.
Kalsbeek, F., Frei, D., Affaton, P., 2008. Constraints on provenance, stratigraphic correlation and structural context of the Volta basin, Ghana, from detrital zircon geochronology: an Amazonian connection? Sediment. Geol. 212, 86–95.
Kalsbeek, F., Frei, R., 2010. Geochemistry of Precambrian sedimentary rocks used to solve stratigraphical problems: an example from the Neoproterozoic Volta basin, Ghana. Precambrian Res. 176, 65–76.
Khanehbad, M., Moussavi-Harami, R., Mahboubi, A., Nadjafi, M., Mahmudy Gharaie, M. H., 2012. Geochemistry of carboniferous sandstones (sardar formation), east-Central Iran: implication for provenence and tectonic setting. Acta Geol. Sin. 86 (5), 1200–1210.
Lang, X.H., Liu, D., Deng, Y.L., Tang, J.X., Wang, X.H., Yang, Z.Y., Cui, Z.W., Feng, Y.X., Yin, Q., Xie, F.W., Huang, Y., Zhang, J.S., 2018. Detrital zircon geochronology and geochemistry of Jurassic sandstones in the Xiongcun district, southern Lhasa subterrane, Tibet, China: implications for provenance and tectonic setting. Geol. Mag. https://doi.org/10.1017/s0016756818000122.
Leube, A., Hirdes, W., Mauer, R., Kesse, G.O., 1990. The early Proterozoic Birimian Supergroup of Ghana and some aspects of its associated gold mineralisation. Precambrian Res. 46, 139–165.
McLennan, S.M., Hemming, S., McDaniel, D.K., Hanson, G.N., 1993. Geochemical approaches to sedimentation, provenance, and tectonics. In: Johnson, M.J., Basu, A. (Eds.), Processes Controlling the Composition of Clastic Sediments, vol. 284. Geological Society of America, Special Paper, pp. 21–40.
McLennan, S.M., Nance, W.B., Taylor, S.R., 1980. Rare earth element-thorium correlations in sedimentary rocks, and the composition of the continental crust. Geochem. Cosmochim. Acta 44 (11), 1833–1839.
McLennan, S.M., Simonetti, A., Goldstein, S.L., 2000. Nd and Pb isotopic evidence for provenance and post-depositional alteration of the Paleoproterozoic Huronian Supergroup, Canada. Precambrian Res. 102, 263–278.
McLennan, S.M., Taylor, S.R., 1991. Sedimentary rocks and crustal evolution: tectonic setting and secular trends. J. Geol. 99, 1–21.
Nesbitt, H.W., Markovics, G., Price, R.C., 1980. Chemical processes affecting alkalis and alkali earths during continental weathering. Geochem. Cosmochim. Acta 44, 1659–1666.
Nesbitt, H.W., Young, G.M., 1982. Early Proterozoic climates and plate motions inferred from major element chemistry of lutites. Nature 299, 715–717.
Nesbitt, H.W., Young, G.M., 1984. Prediction of some weathering trends of plutonic and volcanic rocks based on thermodynamic and kinetic considerations. Geochem. Cosmochim. Acta 48, 1523–1534.
Nesbitt, H.W., Young, G.M., 1989. Formation and diagenesis of weathering profiles. J. Geol. 97, 129–147.
Nesbitt, H.W., Young, G.M., 1996. Petrogenesis of sediments in the absence of chemical weathering: effects of abrasion and sorting on bulk composition and mineralogy. Sedimentology 43, 341–358.
Nude, P.M., Shervais, J.W., Attoh, K., Vetter, S.K., Corey Barton, C., 2009. Petrology and geochemistry of nepheline syenite and related carbonate-rich rocks in the Pan-African Dahomeyide orogen, southeastern Ghana, West Africa. J. Afr. Earth Sci. 55, 147–157.
Oghenekome, M.E., Chatterjee, T.K., Hammond, N.Q., van Bever Donker, J.M., 2016. Provenance study from petrography of the late permian-early triassic sandstones of the balfour formation karoo supergroup, South Africa. J. Afr. Earth Sci. 14, 125–132.
Pettijohn, F.J., 1975. Sedimentary Rocks, third ed. Harper and Row, New York 628pp.
Rollinson, H.R., 1993. Using Geochemical Data: Evaluation, Presentation, Interpretation. Longman Group, UK, pp. 1–315.
Roser, B.P., 2000. Whole rock geochemical studies of clastic sedimentary suites. Memory of Geological Society of Japan 57, 73–89.
Roser, B., Korsch, R., 1986. Determination of tectonic setting of sandstone-mudstone suites using content and ratio. J. Geol. 94 (5), 635–650.
Roser, B., Korsch, R., 1988. Provenance signatures of sandstone mudstone suites determined using discriminant function analysis of major-element data. Chem. Geol. 67 (1–2), 119–139.
Rudnick, R.L., 1992. Restites, Eu anomalies and the lower continental crust. Geochem. Cosmochim. Acta 56 (3), 963–970.
Shervais, J.W., Branney, M.J., Geist, D.J., Hanan, B.B., Hughes, S.S., Prokopenko, A.A., Williams, D.F., 2006. Hotspot: the snake river scientific drilling project tracking the yellowstone hotspot through space and time. Sci. Drill. 3, 56–57.
Taylor, S.R., McLennan, S.M., 1985. The Continental Crust: its Composition and Evolution. Blackwell Scientific Publications, p. 312.
Taylor, S.R., McLennan, S.M., 1995. The geochemical evolution of the continental crust. Rev. Geophys. 33, 241–265.
Taylor, N.P., Moorbath, S., Leube, A., Hirdes, W., 1992. Early Proterozoic crustal evolution in the Birimian of Ghana: constraints from geochronology and isotope geochemistry. Precambrian Res. 56, 97–111.
Tobia, F.H., Aswad, K.J., 2015. Petrography and geochemistry of Jurassic sandstone, Western Desert, Iraq: implications on provenance and tectonic setting. Arab J Geosci 8, 2771–2784.
Toulkeridis, T., Clauer, N., Kröner, A., Reimer, T., Todt, W., 1999. Characterization, provenance, and tectonic setting of fig tree greywackes from the archaen barberton greenstone belt, South Africa. Sediment. Geol. 124, 113–129.
Trompette, R., 1994. Geology of Western Gondwana (2000– 500 Ma). Pan-African-Brasiliano Aggregation of South America and Africa. Balkema, Rotterdam, pp. 1–350.
Verma, S.P., Armstrong-Altrin, J.S., 2016. Geochemical discrimination of siliciclastic sediments from active and passive margin settings. Sediment. Geol. 332, 1–12.
Wang, S., Mo, Y., Wang, C., Ye, P., 2016. Paleotethyan evolution of the Indochina Block as deduced from granites in northern Laos. Gondwana Res. 38, 183–196.
Wronkiewicz, D.J., Condie, K.C., 1987. Geochemistry of Archean shales from the Witwatersrand Supergroup, South Africa: source-area weathering and provenance. Geo. Cosmo. Acta 51, 2401–2416.
Wronkiewicz, D.J., Condie, K.C., 1990. Geochemistry and mineralogy of sediments from the Ventersdorp and Transvaal Supergroups, South Africa: cratonic evolution during the early Proterozoic. Geo. Cosmo. Acta 54, 343–354.
Yang, H., Kyser, K., Ansdell, K., 1998. Geochemical and Appendix A. Locations and mineralogical assemblages of the analysed samples Nd isotopic compositions of the metasedimentary rocks in the La Ronge Domain, Trans-Hudson Orogen, Canada: implications for the evolution of the domain. Precambrian Res. 92, 37–64.